Distribution of Te, As, Bi, Sb and Se in; MORB, Komatiites and in Picrites and Basalts from Large Igneous Provinces: Implications for the Formation of Magmatic Ni-Cu-PGE Deposits

Authors: *Sarah-Jane Barnes[1], Eduardo T. Mansur[12],

[1]Sciences de la Terre, Université du Québec à Chicoutimi, Québec, G7H 2B1, Canada

[2] Present address Norges geologiske undersøkelse, Leiv Eirikssons vei 39 7040 Trondheim, Norway

- Corresponding author Email sjbarnes@uqac.ca

Published as

S.-J. Barnes et E. T. Mansur, "Distribution of Te, As, Bi, Sb, and Se in Mid-Ocean Ridge Basalt and Komatiites and in Picrites and Basalts from Large Igneous Provinces: Implications for the Formation of Magmatic Ni-Cu-Platinum Group Element Deposits," *Economic Geology*, vol. 117, no. 8, pp. 1919-1933, 2022. doi: 10.5382/econgeo.4887.

Abstract

In magmatic nickel-copper-platinum-group element (PGE) deposits the PGE are found both in solid solution in base metal sulfides and as platinum-group minerals (PGM). Apart from S the most common elements that the PGE combine with to form PGM are Te, As, Bi, Sb and Sn (TABS). Whether the TABS play a role in collecting the PGE or simply partition into the sulfide liquid along with the PGE and later combine with PGE when the sulfide phases become saturated PGE is not currently clear. This is in part because the concentrations of TABS in the magmas (picrites and basalts from large igneous province and komatiites) which form these of types of deposits are not well established and hence it is not evident whether the magmas contain sufficient TABS to control PGE. In order to establish the concentrations of Te, As, Bi, Sb and Se (TABS+) in these rock types and to document the processes affecting these concentrations we have determined TABS+ concentrations in komatiites, in MORB and in picrites and basalts from large igneous provinces. Using TABS+

mantle normalized diagrams the affects of; different mantle sources, crystal fractionation, crustal assimilation, degassing and alteration are considered. We estimate the concentrations of TABS+ in komatiites to be approximately twice primitive mantle values. In picrites the concentrations vary from approximately ten times primitive mantle values for As and Sb and decrease through Bi to Te from seven to two times primitive mantle.

Assimilation of S-bearing sedimentary rocks is thought to be important in triggering sulfide saturation leading to the formation of Ni-Cu-PGE deposits. Assimilation of such sediments would enrich the magma in Th over Nb and in As, Sb and Bi. Evidence of assimilation is in the form of TABS and Th enrichment is clear in the PGE reef deposits of the Bushveld and Stillwater Complexes, but the deposits do not contain sufficient TABS to control the PGE. This is also true in the Noril'sk-Talnakh Ni-Cu-PGE deposits. However, at Noril'sk degassing of the magma has resulted in the loss of TABS which results in negative As, Bi, Se and Te anomalies on primitive mantle normalized plots.

Key words: Tellurium, Arsenic, Antinomy, Selenium, Bismuth, platinum-group elements, magmatic ore deposits, crustal assimilation; sulfide segregation; degassing, Siberian flood basalts, komatiites, MORB, Karoo, Etendeka, Emeishan.

Introduction

Tellurium, As, Bi, Sb and Sn (TABS) are essential components of most platinum-group minerals (PGM) found in magmatic Ni-Cu and platinum-group-element (PGE) deposits and hence they may play a role in the formation of these deposits. However, to consider whether they play an active role (i.e. they act as collectors of the PGE; Hanley, 2007; Helmy et al., 2010, 2020; Piña et al., 2015,; Anenburg and Marvogenes, 2016; Cafagna and Jugo, 2016; Liang et al., 2019;) or whether their role is passive (i.e. both TABS and PGE partition from a silicate magma into a sulfide liquid and eventually the sulfide liquid or sulfide minerals becomes saturated in the PGM; Dare et al., 2014; Liu and Brenan, 2015; Duran et al., 2017; Mansur et al., 2020a; Mansur and Barnes, 2020a) it is necessary to estimate their concentrations in the silicate magmas from which the sulfide liquid segregates.

Most Ni-Cu-PGE deposits are found in association with either komatiites or mafic magma of large igneous provinces (Barnes and Lightfoot, 2005; Wilson, 2012; Maier et al., 2013; Barnes et al., 2016; Jenkins and Mungall, 2018). However, because of analytical difficulties there are very few determinations of TABS concentrations in these rock types (Mansur et al., 2020b). Therefore, we have determined the concentrations of Te, As, Bi Sb and Se (hereafter abbreviated to TABS+ to include Se) from 116 samples of; picrites and basalts from large igneous provinces (LIPs), komatiite and MORB. These samples were selected because they have been previously studied and whole rock major and trace element (including S, Cu and PGE) contents were already known.

In this work we show that establishing the initial TABS+ contents of magma that formed these rock types is complex as these elements are affected by numerous competing processes. The MORB lavas show that segregation of sulfide liquid leads to strong depletion of Te, Pd and Pt relative to the other TABS+ and Cu. Contamination with continental crust enriches the magma in Th, As, Sb and Bi relative to Nb, Cu, Se, Te, Pd and Pt. Degassing leads to depletion of As, Bi Se and Te relative to Th, Nb, Cu, Sb, Pd and Pt. Alteration leads to enrichment in As, Sb and Bi. (In this work we use the word alteration to refer to changes in rock composition brought about by either metamorphism or hydrothermalizm). In order to separate these processes, we have developed primitive mantle normalized plots on which the elements are plotted in order of partition coefficient between silicate and sulfide liquid. We then apply these results to modeling the concentrations of TABS+ in the Bushveld and Stillwater PGE deposits and to the Ni-Cu-PGE deposits of Noril'sk-Talnalk district.

Materials and Methods

Materials

The samples are: Komatiites from the Abitibi and Belleterre (Canada) and Barberton (South Africa) Greenstone belts; basalts from the Cape Smith fold belt (Canada); MORB from, the Hotu seamount, the Garret fracture zone and the South Atlantic Ridge; picrites and basalts from the Siberian, Emeishan, Etendeka and Karoo LIPs (Fig. 1.) The samples were chosen because they had been previously investigated to understand their PGE content. More details on the samples can be found in electronic supplementary materials 1 (App.1).

Analytical Methods

Tellurium, As, Bi, Sb and Se analyses were carried out by Hydride Generation-Atomic Fluorescence Spectrometry (HG-AFS) following the technique described by Mansur et al. (2020b), at LabMaTer Université du Québec à Chicoutimi (UQAC). International reference materials (CH-4 and TDB-1 from Natural Resources Canada and OKUM from IAGEO), and a blank were determined at the same time as the samples. The detection limits based on 3σ of the blank are 0.005, 0.003, 0.005, 0.005 and 0.002 ppm for Te, As, Bi, Sb and Se, respectively. The results for the reference materials agree with working values (App 2 Table A1).

For most samples, whole-rock analyses were already available in the original publications. For samples where they were not, the samples were analyzed at LabMaTer, (UQAC) by LA-ICP-MS details in Appendix 1 The certified reference materials OKUM, KPT-1 (IAG reference materials), WPR-1 (CANMET) and UB-N (CNRS-CRPG), were used to monitor the results. The results obtained for the reference materials agree with the working values (App 2, Table A2).

Rational for the use of primitive mantle normalized plots

The data is presented on primitive mantle normalized diagrams. The mantle normalization factors used were those of Lyubetskaya and Korenaga (2007). Wang et al. (2018) provide more recent estimations based on a combination of Lyubetskaya and Korenaga (2007), McDonough and Arevalo (2008) and Palme and O'Neil (2014) and a statistical approach to minimize errors. Estimations of the concentrations of TABS+ in the primitive mantle are poorly constrained because of the many processes affecting their distribution and analytical difficulties. The concentrations of As, Sb and Bi in these publications are based on the ratios of these elements to Pb or Ce in ocean floor basalts and concentrations of Se and Te are based on the ratio of these elements to S in CI chondrites. Wang's et al. (2018) estimations are within error the same as those of Lyubetskaya and Korenaga (2007) for the elements considered here and the shape and level of the patterns presented would not significantly change if Wang et al.'s (2018) values were used.

In the crust and mantle the TABS+ behave as chalcophile elements (i.e. they partition into base metal sulfide liquid and minerals; Hattori et al., 2002; Patten et al., 2013; Brenan, 2015; Li and Audétat, 2015; Liu and Brenan, 2015; Greaney et al., 2017). Therefore, during partial melting of the mantle the presence of sulfides in the restite may deplete the magma in TABS+, and the segregation of a sulfide liquid during transport of crystallization will have a similar effect. However, the TABS+ are not equally chalcophile. Arsenic and Sb are slightly chalcophile ($D^{Sulf\ liq/Sil\ liq}$ <10), Bi, Se and Cu are strongly chalcophile ($D^{Sulf\ liq/Sil\ liq}$ from 100 to 1000) and Te is highly chalcophile ($D^{Sulf\ liq/Sil\ liq}$ >1000) (Barnes, 2016 and references therein). Thus, the TABS+ may be fractionated from each other by segregation of a sulfide liquid. In order to assess the effect of sulfide liquid segregation or sulfide liquid accumulation the elements are arranged in order of partition coefficient into a sulfide liquid (Fig. 2A).

Sulfides are not always present during partial melting and crystallization, which is important because the TABS+ are incompatible with most mafic minerals (Kamenetsky and Eggins, 2012; Jenner and O'Neill, 2012; Maciag and Brenan, 2020; Mansur and Barnes, 2020b) and thus should correlate with lithophile incompatible elements. To take into consideration the effects of degree of partial melting and/or crystal fractionation Th, Nb (or Ta) were added to the diagram as representatives of the lithophile incompatible elements (Fig. 2A)

Contamination of mafic magmas by continental crust is common, and the continental crust, and in particular black shale, is enriched in As, Sb and Bi (Fig. 2B; Ketris and Yudovich, 2009; Godel et al., 2012; Piña et al., 2013, 2015; Samalens et al., 2017; Le Vaillant et al., 2018). Thus, contamination with continental crust results in enrichment in As, Sb and Bi as has been previously shown for the Bushveld Complex B-1 dikes (Mansur and Barnes, 2020b Fig. 2B). Thorium is also enriched in continental crust rocks, thus if a magma has experienced contamination by continental crust a negative Nb or Ta anomaly is observed (Fig. 2B).

The TABS+ and S are volatile (Lodders, 2003; Wood et al. 2019), and therefore subaerial lavas could be depleted in these elements during degassing (Iacono-Marziano et al., 2012, 2017; Zelensky et al., 2014; Mather et al., 2015; Forrest et al., 2017; Edmonds and Mather, 2017; Edmonds et al., 2018; Cox et al., 2019; Wiesener et al., 2020). In order to take this into consideration, chalcophile elements that are less volatile (Cu, Pd, and Pt) were added to the plot at the position of their relative partition coefficients into base metal sulfide liquid. If degassing has occurred one would predict that there should be depletion of the TABS+ relative to Cu, Pd and Pt (Fig. 2A).

Finally, it is well established that the TABS+ can be mobilized either during metamorphism (Pitcairn et al., 2015; Hammerli et al., 2016) or hydrothermal activity (Guo and Audétat, 2017; Patten et al., 2017; Stucker et al., 2017; Shevko et al 2018;). Deviations from the trends shown by the immobile elements may be the result of alteration.

Results and Interpretation

The overall geochemical characteristics of samples from the various localities are presented using primitive mantle normalized plots (Fig. 3). Median values for each locality are presented in (Table 1). The plots for individual samples are shown in the Appendix 3 (Fig. A1 and A2). The individual whole-rock results can be found in Table A3.

MORB

The MORB samples show two slightly different primitive mantle normalized patterns (Fig. 3A). The patterns for samples from the South Atlantic Ridge and the Garret Fracture Zone display a typical N-MORB shape, with relatively flat slopes from Th to Se at approximately 1-10 times primitive mantle, followed by steep negative slopes from 0.5-2 times primitive mantle at Te to 0.001-0.1 times primitive mantle at Pt. The E-MORB samples have higher Th and Nb contents at 10 to 40 times primitive mantle but have similar pattern to N-MORB samples for the chalcophile elements (Fig. 3A). Jenner and O'Neill (2012) reported similar results for As, Bi, Sb, Cu and Se for a large dataset of MORB glasses, whereas Yi et al. (2000) reported results for Te which are slightly lower than ours (0.001 to 0.01 ppm vs <0.005 to 0.014 ppm).

Patten et al. (2013) reported on the presence of sulfide droplets in these samples and modelled the strong Pt and Pd depletion by the segregation of an immiscible sulfide liquid during crystal fractionation. However, the relatively flat primitive mantle normalized patterns of the N-MORB samples from Th to Se do not show evidence of sulfide segregation. This is because, it is the bulk partition coefficients ($D^{sulf\ liq/sil\ liq}$ * weight fraction of sulfide liquid segregated) that controls the behavior of the elements. If the MORB samples originally contained Pd and Pt at the same levels as Th to Se, (~3 times primitive mantle), only a very small amount of sulfide liquid needs to have segregated to lower the concentrations of Te through to Pt to their current levels. Assuming saturation of the basalts at 1000 ppm S and allowing for ten percent equilibrium fractionation with cotectic segregation of the sulfide liquid, the Pd and Pt concentrations would be lowered to the median levels seen in our MORB samples. The concentrations of Te with its high partition coefficients into sulfide liquid ($D^{sul\ liq/sil\ liq}$ >5000; Patten et al., 2013; Liu and Brenan, 2015) would be similarly affected. In contrast, because of the lower partition coefficients of the other chalcophile elements they are only slightly affected (model line on Fig. 3A).

Here we have modelled the depletion of Te, Pd and Pt as though it occurred in the oceanic crust because the samples contain sulfide droplets and were sulfide saturated. If, on the other hand, a small amount sulfide remained in the mantle source during partial melting the result would be the similar.

The incompatible elements Th and Nb are markedly enriched in E-MORB (Fig. 3A) relative to the chalcophile elements. This suggests that whereas an E-MORB source is enriched in incompatible lithophile elements it is not enriched in chalcophile elements and that this enrichment is not due in continental crustal component as both Th and Nb are enriched.

Cape Smith

The Cape Smith basalts have an almost flat pattern at 2 to 6 times primitive mantle. Antinomy and Bi are slightly enriched relative to the other elements. The levels of Th, Nb, Bi, Cu, Se are similar to N-MORB, but the levels of the highly chalcophile elements Te, Pd and Pt are much higher than MORB (Fig. 3B). These basalts have been modeled as the product of approximately 20% partial melting of the mantle and very little retention of sulfide minerals in the mantle (Barnes and Picard, 1993). Assuming a primitive mantle source the TABS primitive mantle normalized pattern in this case should be essentially flat at 5 times primitive mantle (Fig. 3B) with no depletion in Te, Pd and Pt. The median TABS patterns match the model pattern except for the enrichment of Sb and Bi. This enrichment could be the product of seafloor alteration, as these elements have been shown to be mobile during seafloor alteration (Patten et al., 2017). But it could also have occurred during metamorphism as the rocks have experienced greenschist facies metamorphism (Picard et al., 1990). Pitcairn et al. (2015) showed that As and Sb can be enriched in basalts that have undergone lower greenschist facies metamorphism (Bi was not included in their study).

Komatiites

The Al-undepleted komatiites from the Abitibi and Belleterre Greenstone belts display similar patterns, which, with the exceptions of As, Sb and Bi, are relatively flat at 1 to 6 times primitive mantle. The samples have positive As, Sb and slight Bi positive anomalies at 8 to 30 times primitive mantle (Fig. 3C).

Based on the depletion of highly incompatible elements (La, Zr and Hf), which show a depletion factor of ~0.6 relative to moderately incompatible elements, Barnes et al. (1983) modelled the Alexo komatiites as the product of 25 to 40% partial melt of depleted mantle. The concentrations of Th and Nb at one times primitive mantle are consistent with this model (Fig. 3C). The level of Cu through to Pt at approximately two times primitive mantle is similar to that of primitive mantle for the moderately incompatible elements (Sm, HREE and TiO_2) for these rocks. We interpret this to be because the elements Cu to Pd behaved as moderately incompatible elements during the earlier partial melting event which initially depleted the komatiite source in highly incompatible elements.

The Al-depleted komatiite samples from the Barberton Greenstone Belt also show enrichment in As, Sb and Bi. The Al-depleted komatiites but are relatively depleted in the other chalcophile elements which are mostly present at less than one time primitive mantle (Fig. 3D). The Hooggenoeg Formation samples are enriched in Th relative to Nb (Fig. 3D).

The depletion of Cu, Se, Te, Pd and Pt could be due to segregation of a sulfide liquid. However, Maier et al. (2009) argued that the low concentrations of PGE in these rocks and other komatiites of the early Archean is due to the mantle source being depleted in PGE due to incomplete mixing of the late veneer. One of three formations (the Hooggenoeg) is enriched in Th over Nb suggesting that the Hooggenoeg samples have experienced crustal contamination.

All of the komatiites are enriched in As, Sb, and Bi relative to the other elements at 10 to 20 times primitive mantle (Fig. 3C and D). This enrichment is not thought to be due to crustal contamination because Th is not enriched relative to Nb (except in the Hooggenoeg

Formation). Neither is the enrichment thought to be due to enrichment in the komatiite mantle source because these elements do not behave in a coherent fashion. For example, at Alexo (where the komatiites showing the lowest degree of metamorphism and alteration of the komatiites) a plot of Nb versus Mg# shows a typical trend for incompatible element with Nb increasing as Mg# drops, and the spinifex-textured and chill samples (+) having higher Nb values than the olivine-rich (o) lower parts of the flows (Fig. 4A). In contrast, Sb, As and Bi concentrations do not correlate with Mg# (Bi distribution shown in Fig. 4B). As mentioned above basalts that have undergone greenschist metamorphism are enriched in As and Sb (Pitcairn et al. 2015) thus the enrichment of As, Sb and by analogy Bi in the komatiites could be the result of metamorphism.

Large Igneous Provinces

Most of the samples from LIPS show similar patterns with overall negative slopes decreasing from Th and Nb (primitive mantle normalized values in the 10 to 70 range) to Pd and Pt values in the 1-3 range (Fig. 3E to H). The Nd lavas from the Siberian province are an exception containing even lower values of Pd and Pt. Most samples from LIPs also show negative As, Bi, Se and Te anomalies (Fig. 3E to H), with the exceptions that Dali picrites and the Etendeka dikes which do not show Bi anomalies (Fig. 3E and F).

The patterns from different localities, do however, show differences in Th to Nb ratios. Most of the Emeishan samples, the picrite dikes from Etendeka and the picrite from Tuli (Karoo) do not show Th enrichment over Nb, (Figs. 3E, F and G). In contrast, rocks from almost all of the other Karoo formations and the Siberian lavas are enriched in Th (Fig. 3G and H).

The patterns of the LIPs rocks are more complex than those of MORB and komatiites where a combination of differences in mantle source, sulfide segregation and alteration were sufficient to explain the patterns. In the case of LIPs degassing and continental crustal contamination must be considered. These samples were not metamorphosed or hydrothermally altered so alteration not as important as in the case of the komatiites.

Degassing The most striking difference between the sub-aqueous rocks (MORB, Cape Smith and komatiites) and LIPs rocks are the negative As, Bi, Se, and Te anomalies. We attribute these anomalies to magma degassing for the following reasons: i) The low Se and Te values cannot be attributed to sulfide segregation because Se has similar partition coefficient to Cu into sulfide liquid and thus would be expected to be present at similar levels to Cu. Similarly, Te has a slightly lower partition coefficient into sulfide liquid than Pd and thus would be expected to be present at a higher or similar level to Pd; ii) The anomalies are not due to continental crust contamination because as will be discussed below this would enrich the magmas in As, Sb and Bi rather than depleting them; iii) The lavas contain vesicles indicating gas loss; iv) Sub-aqueous mantle derived magmas generally contain 1000 ppm S whereas most of our LIPs rocks contain <100 ppm indicating S loss; and v) Like S, the TABS+ are volatile (Lodders, 2003; Wood et al., 2019) thus are prone to loss during degassing.

Zelenski et al. (2014) report partition between gas and basalts from Erta Ale, Tolbachik and Kudryavy volcanoes in the 2 to 1000 range for As, Bi, Se, and Te. For Cu, Sb and Pt the partition coefficients are in the 0.001 to 0.1 range (Fig. 2A). Zelenski et al. (2014) do not report partition coefficients for Th or Nb, however given their low volatility (Loedders, 2003; Wood et al., 2019) they would not be expected to partition into a gas. The difference in the partition coefficients between gas and silicate liquid for As, Bi, Se, Te and Sb, Cu and Pt could explain the negative anomalies for As, Bi, Se and Te. These observations should be tempered with consideration that in some studies Cu, Sb and Pt have been found to be moderately volatile (Mather, 2015). The differences in behavior reported by Zelenski et al. (2014) and Mather (2015) could in part be the result of differences in the oxidation state of the magma (the TABS+ can adopt a range of oxidation states, (Pokrovski et al., 2013)) which could affect their affinity with the gas versus the magma. It is also important to consider when degassing occurred relative to the phases present in the magma (Edmonds and Mather, 2017). Of particular importance is the presence of sulfide liquid and aqueous fluids into which the TABS could also preferentially partition and thus not partition into the gas. In any event, all the TABS+ except Sb appear to have been lost from the LIPs samples.

Continental Crust Contamination. Contamination of the magmas with continental crust or sediment would enrich the samples in As, Sb and Bi (Fig. 2B and 3H). This enrichment could potentially obscure the effects of degassing. For example, consider the Etendeka picrite with a flat pattern but negative As, Se and Te anomalies (Fig. 5A). Contamination with ~ 20% upper continental crust accompanied by 60% crystal fractionation produces a pattern that matches the most evolved Etendeka dolerite sample. The dolerite does not show negative As, Bi or Te anomalies because the continental crust has added sufficient of these elements to eliminate the anomalies. However, there is still a negative Se anomaly because the continental crust does not contain much Se (Hu and Gao, 2008).

Most of the Karoo basalts and dolerites are enriched in Th relative to Nb, which is in agreement with previous work (Marsh et al., 1997) that showed that lavas from these areas have assimilated upper continental crust material. The Tuli basalts can be modeled by 10% crustal contamination of the Tuli picrite (Fig. 5B). The Lesotho and Barkley East basalts have Nb and Th contents lower than the Tuli picrite making this picrite an unsuitable parental magma for these basalts. A magma similar to the Etendeka picrite would be a suitable parental magma. Ten percent crustal contamination of the Etendeka picrite accompanied by 20% crystal fractionation would produce a TABS+ pattern similar to the Lesotho and Barkley East Karoo basalts (model line in Fig. 3G), except that the Karoo basalts show a negative Bi anomaly. Possibly, the Karoo basalts have experienced greater degassing than the Etendeka rocks, which are dikes.

As in the case of the Karoo basalts the Siberian basalts are all enriched in Th over Nb which is in agreement with Lightfoot et al. (1993) that they have experienced continental crust contamination. The Morongovsky (Mr), Mokulaevsky (Mk) and Kharaelakhsky (Kh) formations are similar to the Lesotho and Barkley East Karoo basalts and can be modelled by in a similar manner by contamination with approximately 5% upper continental crust accompanied by 7% crystal fractionation (Fig. 3H). The Nd lavas are more enriched in Th relative to Nb and require a greater degree of contamination (26 %) accompanied by a greater amount of crystal fractionation (30%). More strikingly they show strong depletion from Cu to Pt. These lavas are believed to have been depleted in chalcophile elements due to the segregation of sulfide liquid (Lightfoot et al., 1993; Brügmann et al., 1993; Lightfoot and Keays, 2005). Assuming that the lavas originally contained a similar amount of Pd and Pt to the Mr/Kh lavas only a small amount of sulfide liquid would need to have segregated to lower the Pd and Pt values. If cotectic proportions of sulfides segregated in the last 3% of crystal fractionation the Pd and Pt concentrations would have been reduced to Nd levels (Fig. 3H).

Discussion

The Nature of the Mantle Sources

The Al-undepleted komatiites and Cape Smith basalts contain Se, Te, Pd, and Pt at approximately slightly higher levels than Th and Nb for the komatiites and similar levels for the Cape Smith basalts. We interpret this to imply a slightly depleted mantle source for the komatiite and an undepleted mantle source for the Cape Smith Basalts with no sulfide phase retention. The N-MORB contain Th, Nb, As, Sb, Bi, Cu and Se at approximately similar primitive mantle levels. Given that the N-MORB mantle is depleted in highly incompatible elements we interpret this to indicate that degree of As, Sb, Bi Cu and Se depletion in the N-MORB mantle is similar to that of highly incompatible elements.

All of the LIPs picrites are enriched in the highly incompatible elements Th and Nb relative to the chalcophile elements (Fig. 6). The exact nature of the mantle from which the magmas of LIPs form is a much-debated topic with views ranging from formation by partial melting of a source consisting of primitive mantle, MORB and sediment (Zhang et al., 2019) to formation by partial melting of metasomatized sub-continental lithosphere (Kamenetsky et al., 2012; Shellnutt, 2013). Most of the picrites, (Fig. 6) do not show enrichment in Th over Nb and the TABS+ (the Binchuan picrites are an exception showing slight Th enrichment). The picrites TABS+ patterns however are not all the same and can be divided into two groups based on their Th and Nb contents. The Dali and Etendeka picrites show much lower Th and Nb contents at 10 times primitive mantle than the other Emeishan picrites and the Tuli picrite (Karoo), which contain approximately 30 times primitive mantle levels of Th and Nb indicating a much more enriched source for these picrites (Fig. 6). As in the case of N-MORB vs E-MORB this enrichment in Nb and Th in the Tuli and Emeishan picrites vs the Etendeka and Dali picrites, does not apply to the chalcophile elements (Figs. 3A and 6). This suggests that the process that enriched the sources of E-MORB and many LIPs picrites in Th and Nb did not enrich them in chalcophile elements. Furthermore, the component leading to the enrichment of Th and Nb is not a subducted sediment, as Th is not enriched over Nb.

As pointed out by Zhang et al. (2019) the high Mg# of the Emeishan picrites requires a high degree of melting of a peridotite source. A high degree of partial melting of a peridotite source is consistent with the Pd and Pt concentrations observed in the picrites at 1 to 2 times primitive mantle. On the other hand, the high concentrations of Nb at 10 to 30 times primitive mantle, Sb and Cu primitive mantle normalized levels at 5 and 10 times mantle would require a low degree of partial melting if the mantle source was similar to primitive mantle. The added component that enriched the mantle source must then: i) Not dilute the MgO content of the source, in order to keep the high Mg# of the picrites, therefore it must be a small volume; ii) Be very rich in **both** Th and Nb, i.e. not a sediment or melt of a sediment; iii) Contribute some Cu and Sb; and iv) Probably contribute some As, Bi, Se, Te, however, as these elements are partially lost in subsequent degassing this is not a firm requirement. Exactly what is the nature of this component is not clear to us, but possibly a carbonate melt or fluid might be suitable (e.g. Holwell et al., 2019; Blanks et al., 2020).

Estimation of TABS+ concentrations in komatiite and LIPs magmas

The motivation for this study was to estimate the initial TABS+ concentrations in komatiite and LIPs magmas because these types of magmas are thought to host magmatic Ni-Cu-PGE deposits. Simply calculating the average of TABS+ values for komatiites and LIPS rocks is not sufficient to estimate these concentrations because of the various processes that have modified them. The reasoning for the choice of values are proposed here discussed as below.

The Al-undepleted komatiites and Cape Smith basalts show similar primitive mantle normalized concentrations for Cu, Se, Te, Pd and Pt at approximately 2 and 5 times primitive mantle, respectively, consistent with sufficiently high degrees of partial melting (40% and 20%, respectively) to dissolve all the sulfide minerals in the source and release these elements into the melt. Based on these observations the concentrations of Se and Te in Al-undepleted komatiite can be estimated as approximately twice primitive mantle (Table 2).

Bismuth and Sb are present at higher levels than Th, Nb and the other chalcophile elements in the komatiites and the Cape Smith basalts. This is attributed to metamorphism of the samples and hence the concentrations of Bi and Sb cannot be empirically estimated. Similarly, As in the komatiites is higher than Th, Nb and other chalcophile elements and this could be due to enrichment during metamorphism. However, As is present in the Cape Smith basalts at the same level as Nb and Cu, at five times primitive mantle, and could be primary.

Our N-MORB samples have a median Mg# of 0.65 and hence are close to primary magmas. Thorium, As, Sb, Bi, Cu and Se are all present at approximately 3 times primitive mantle levels and provide a rational for estimating the As, Sb and Bi concentrations in komatiites by assuming that they are present at the same primitive mantle levels as Th, Cu and Se, i.e. twice primitive mantle (Table 2).

Most LIPs picrites appear to be depleted in TABS+ (except Sb) relative to the less volatile elements on the primitive mantle normalized plots. We attribute this depletion to degassing. To estimate the concentrations of the TABS+ before degassing the primitive mantle ratios of Cu/Bi, Cu/Se and Pd/Te could be used. (Assuming Cu and Pd were not significantly depleted during degassing). Based on the similarity of TABS primitive mantle normalized concentrations in N-MORB and for Te and Se in komatiites and the Cape Smith basalts, the original concentrations in the picrites can be estimated by using the adjacent elements. Copper is present at approximately 5 times primitive mantle allowing an estimate for Bi and Se of 5 times primitive mantle and Pd is present at twice primitive mantle allowing an estimate for Te at twice primitive mantle (Table 2).

In the Dali and Etendeka picrites the Th, Nb, Sb levels are approximately the same at 10 times primitive mantle, which implies that the As content should also be 10 times primitive mantle. Estimating the As content for the other picrites is more difficult because Th and Nb are markedly enriched at approximately 30 times primitive mantle, whereas Sb is present at approximately 10 times primitive mantle, as observed for the Dali and Etendeka picrites. In E-MORB, As is present at the same primitive mantle level as Sb, Bi and Cu at 3 times primitive mantle rather than the more than 10 times primitive mantle observed for Th and Nb. Therefore, to estimate the concentration of As in the picrites we have used the primitive mantle concentration of Sb at 10 times primitive mantle (Table 2).

Application to Ni-Cu-PGE Deposits

PGE Deposits The main PGE ore deposits are the Merensky reef, the Platreef, the UG2 reef (all of the Bushveld Complex), the JM reef of the Stillwater Complex and the Main Sulfide zone of the Great Dyke (Naldrett, 2011; Zientek, 2012). Very limited data is available for the UG2 reef and the Main Sulfide zone and they will not be considered here. The primitive mantle normalized plot for the normal and thin reef from the Merensky and JM reef both show an enrichment of Th (at thee to ten times primitive mantle) over Nb and Ta (at 0.1 to 1 times primitive mantle) (Figs. 7A and C). (Data from Mansur and Barnes 2020). This is consistent with the magmas having been contaminated with continental crust. The levels of the patterns increase steadily from approximately one times mantle at As through to approximately 100 times primitive mantle at Bi. The patterns show a slight dip through Cu to Te and then increase markedly to 1000 to 10 000 times primtive mantle (Figs. 7A and C).

The increase in chalcophile element contents from As through to Pt is consistent with the increase in partition coefficients between sulfide and silicate liquid (Liu and Brenan, 2015). The slight Bi anomaly is the product of the much higher partition coefficient for Bi than for Sb between sulfide and silicate liquid and the enrichment of Bi over Cu in the magma due to the contamination of the magma with continental crust (Fig. 2B). The distribution of the chalcophile element content of the normal and thin Merensky reef at Impala and Rustenburg mines have been modelled in detail using a magma of similar composition to the marginal chills of the Bushveld (Mansur and Barnes, 2020b). On average, a model consisting of 2 weight percent sulfide liquid formed at an R-factor of 30 000 and 20 percent trapped liquid component models the composition of these rocks (Fig. 7A). Thus the PGE content of the Rustenburg and Impala normal and thin reefs can be modelled based by collection of PGE and TABS from a silicate magma by sulfide liquid and do not require TABS to collect the PGE.

In addition to the previously published data for the Merensky reef a composite sample, SARM-7, prepared by National Institute of Metallurgy South Africa from 7.5 tonnes of Merensky reef from 4 of the mines of the western limb of the Bushveld, (Steele et al., 1975) was also analyzed. The pattern for a composite sample from the Merensky reef is slightly different to the Impala and Rustenburg normal and thin reef in that it is an order of magnitude richer in both As and Sb (Fig. 7B). This is not an exception. Scanning the results reported for reference materials by African Mineral Standards for Merensky reef samples shows that these are also enriched in As and Sb (Fig. 7B). All of these samples are described on their certifcate of analyses as composite samples from Anglo American mines from the western limb of the Bushveld Complex. Furthermore, reference material from African Mineral Standard for the samples from the Mogalakwena mine of the Platreef also show As and Sb enrichment (Fig. 7B).

In the case of the Merensky reef it is worth considering that in addition to normal and thin reef there are a number of other facies; contact reef, pothole reef, rolling reef, wide reef (Viljoen, 1999). The pothole reef in particular is thought to be associated with the migration of fluids (Kinloch, 1982; Boudreau, 1992; Viljoen, 1999). It is possible that composite samples included some of the pothole reef facies and that the high Sb and As were introduced by the migrating fluids. Against this is the observation that Roberts et al. (2007) showed that the potholes have similar whole rock compositions to normal reef for most elements (although they did not determine the TABS+ concentrations). Roberts et al. (2007) argued that the potholes are product of magmatic slumping and that fluids have not substantially altered the composition of the potholed reef. The high As and Sb concentrations in the composite samples and particularly in the case of the Platreef may be the product of the magma having been locally contaminated with rocks such as a black shale, which could have contributed more As and Sb to the magma than observed in the average chill samples used for the modeling (Fig. 2A).

TABS+ analyses of the chilled margins of the Stillwater are not available. However, it is thought that the magmas from which the Stillwater formed are similar to the Bushveld complex (Barnes et al., 2020). The modeled values of the chalcophile elements from the Merensky reef are shown for comparison on Fig. 7B. The model composition of the Merensky reef is similar to that of the JM reef for most chalcophile elements. However, as is well known Pd is far more enriched in the JM reef than the Merensky reef.

A number of reasons have been proposed for the high Pd content. Most recently, Jenkins et al. (2020) proposed that the sulfides formed in equilibrium with a more fractionated magma at very high R-factors (50 000 to 500 000). The increase in R-factor could account for the higher Pd concentrations in the JM reef while not affecting the concentrations of most of the elements because the partition coefficients of most of the chalcophile elements are less than 10 times the R-factor (Campbell and Barnes, 1984). In order to explain the observation that Pt is not as enriched as Pd (as would be expected given its high partition coefficient between silicate and sulfide liquid) they argue that fO_2 was low (FMQ-1.5) and thus Pt had crystallized from the magma by the time sulfide saturation was achieved. One difficulty with this model is the large quantity of magma required, where and how the magma and sulfide liquid interacted is not considered in Jenkins et al. (2020). Barnes et al. (2020) considered a number of models to account for the high Pd and high R-factor and concluded on balance that the magma became contaminated with a continental crustal component either at the margins of the intrusion or at depth and that the sulfides interacted with a large volume of magma either as it slumped into the magma chamber from the margins or if sulfide saturation occurred at depth as the magma was transported into the chamber resulting in upgrading of the sulfides during transport.

The main alterative model favored by Boudreau (2016) is that late magmatic fluids partial dissolved disseminated magmatic sulfides in the cumulate rocks underlying the reef. The more soluble chalcophile elements, and in particular Pd, dissolved in the fluid. The fluid rose until it reached fluid understatured magma where it dissolved into the magma. The S and chalcophile elements transported by the fluid precipitated as base metal sulfide and form the reef. Relevant experimental data to model this process for the TABS+ is not available.

*Noril'sk-Talnakh Nickel-Copper Deposits*_The Noril'sk-Talnakh ore camp of Siberia is the largest or second largest magmatic Ni-Cu deposit in the world (Naldrett, 2011). The massive sulfide ores are mineralogical and compositionally zoned (Distler, 1994; Sluzhenikin et al., 2014). Duran et al. (2017) classified the sample set of massive ores considered here into: i) Cu-poor (chalcopyrite cubanite-poor <10%; with pyrrhotite>70%); ii) Cu-rich (chalcopyrite-cubanite-rich >50%, with pyrrhotite <10%); and iii) transitional ores for those that contained intermediate amounts of pyrrhotite and chalcopyrite. Pentlandite concentrations in the ore types are relatively constant at 10 to 30%. The zonation is thought to be the product of crystal fractionation of the sulfide liquid with the Cu-poor ores representing the early formed cumulates and Cu-rich ores forming from the fractionated liquid (Distler, 1994; Duran et al., 2017).

The ores are found associated with three intrusions, Noril'sk I, Talnakh and Kharaelakh. The primitive mantle-normalized patterns for all ore types are similar (Fig. 8).

They show a steep increase from As in the 10 times mantle range through to Cu in the 1000 (Cu-poor ore) to 10 000 times mantle range (Cu-rich ore) followed by negative Se and Te anomalies, both elements being present at five to ten times less than Cu primitive mantle levels (Figs. 8A to D). In the ores from Kharaelakh and Talnakh Pd is present at approximately the same level as Cu, whereas in the Noril'sk I ores Pd is enriched by almost an order of magnitude. Mantle normalized levels of Pt at all localities are approximately five times lower than Pd.

All of the TABS+, are strongly incompatible with the first mineral (monosulfide solid solution, MSS) to crystallize from the sulfide liquid, an exception to this is Se which is only slightly incompatible (Helmy et al., 2010; Lui and Brenan 2015; Sinyakova et al., 2017). Thus, although the primitive mantle normalized patterns may vary in level, the shape of the patterns should be similar throughout the ore types, reflecting the trapped liquid component. This can be observed for the ores associated with the Talnakh and Kharaelakh intrusions, with the Cu-poor ores having the lowest the levels of TABS+ and the Cu-rich ores having the highest levels, and transitional ores having intermediate levels (Figs. 8A to C). For the Noril'sk I ores, TABS+ are only available for the transitional and Cu-rich ores (Fig. 8D). However, the same observations can be made that the median patterns for Cu-rich ore and transitional ore are similar, and the Cu-rich ore is enriched in TABS+ relative to the transitional ore.

Assuming that the silicate magma from which the sulfides segregated was similar in composition to the Mr/Kh lavas the composition of the sulfide liquid at Kharaelakh and Talnakh can be modelled using an R-factor of 1 000 (consistent with previous estimates used to model the PGE and Cu contents of the rocks; Duran et al., 2017). The primitive mantle-normalized pattern of the model approximates the shape of the patterns for the ores except the model does not show as strong a depletion in Pt relative to Pd. Platinum is known to crystallize under reducing conditions (Canali et al., 2017) and is possible that the magma from which the sulfides segregated had crystallized some Pt prior to sulfide segregation.

The model reproduces the negative Se and Te anomalies found in all ore types. Given that the concentrations of these elements in the lavas appeared to be depleted due to degassing we suggest that the magma from which the sulfides segregated was also depleted in Se and Te due to degassing. Iacono-Marziano et al. (2012, 2017) in their studies of the Noril'sk-Talnakh ores considered that degassing occurred during the formation of Norilsk-Talnakh ores as consequent of crustal contamination and in fact the process was common throughout the Siberian LIP.

The Noril'sk I ores have been modelled with higher R-factors. Using an R-factor of 10 000 the TABS+ primitive mantle pattern approximates the observed patterns. In fact, because most of the TABS+ have $D^{sul/sil\ liq}$ <1000 the TABS+ pattern at R=1 000 and R=10 000 is the same for As through to Bi. The difference is only evident from Cu onwards. As in the case of the Kharaelakh and Talnakh ores the Noril'sk I ores also show Se and Te negative anomalies, which we attribute to the magma having degassed.

Conclusions

We investigated the distribution of TABS+ in picrites and basalts from LIPs, komatiites and MORB. Our main findings are summarized as follows:

1- Primitive mantle normalized plots can be used to consider the processes that affect the distribution of TABS+.
2- Komatiites contain Se and Te at the same primitive mantle level as Pd, Pt and Cu, and slightly higher than in the primitive mantle level of the highly incompatible elements Th and Nb. This is consistent with derivation from a slightly depleted mantle source with no sulfide phase retention during partial melting.

3- N-MORB contain As, Sb, Bi, Cu and Se at the same level of enrichment relative to primitive mantle as Th, consistent with a depleted mantle source.

4- N-MORB are strongly depleted in Te, Pd and Pt, but not the other TABS and Cu. This is consistent with segregation of a small amount of sulfide liquid.

5- E-MORB is similar to N-MORB with respect to the TABS+ and PGE, but enriched in Th and Nb requiring a source that is not enriched in TABS, but is enriched in Th and Nb.

6- The LIPs picrites are enriched in Th and Nb relative to the TABS+, Cu, Pd and Pt. This enrichment combined with the high Mg# requires a peridotite source that has been preferentially enriched with a small amount of a fluid or magma very rich in Th **and** Nb, possibly a carbonatite.

7- Some LIPs basalts are enriched in Th over Nb due to assimilation of continental crust. This would have also enriched the magmas in As, Sb and Bi. However, degassing has led to the loss of As, Bi, Se and Te. Antimony does not appear to have been significantly lost.

8- The initial concentrations of TABS+ in the magmas (komatiites and LIPs) from which major Ni-Cu-PGE deposits form can be estimated as approximately twice primitive mantle for komatiites and between 10 for As and Sb though 7 to 2 times primitive mantle from Bi to Te for LIPs picrites.

9- The TABS+ and PGE contents of normal and thin Merensky reef and JM reef can be modelled by collection of both TABS+ and PGE by a magmatic sulfide liquid in equilibrium with a komatiitic magma contaminated with continental crust and do not require TABS to collect the PGE.

10- The TABS+ concentrations in Noril'sk- Talnakh Ni-Cu deposits can be modelled as being in equilibrium with a mafic magma that had been contaminated with continental crust and which was also depleted in TABS+. This implies that the magma was degassed or degassing at the time that the sulfides formed.

Acknowledgements

This work was supported by a Canada Research Chair program grant to Sarah-Jane Barnes (215503) and Discovery Grant 1884-2013. This manuscript benefited from insightful comments from the reviewers, Drs. Giada Iacono-Marziano and *Steve Barnes and careful editorial handling by the editors.*

References

Anenburg, M., and Mavrogenes, J. A., 2016, Experimental observations on noble metal nanonuggets and Fe-Ti oxides, and the transport of platinum group elements in silicate melts: Geochimica et Cosmochimica Acta, v. 192, p. 258-278.

Arguin, J.-P., Pagé, P., Barnes, S.-J., Yu, S.-Y., and Song, X.-Y., 2016, The effect of chromite crystallization on the distribution of osmium, iridium, ruthenium and rhodium in picritic magmas: an example from the Emeishan Large Igneous Province, Southwestern China: Journal of Petrology, v. 57, p. 1019-1048.

Barnes, S.-J., 2016, Chalcophile Elements, *in* White, W. M., ed., Encyclopedia of Geochemistry: A Comprehensive Reference Source on the Chemistry of the Earth: Cham, Springer International Publishing, p. 229-233.

Barnes, S.-J., and Lightfoot, P. C., 2005, Formation of magmatic nickel sulfide ore deposits and processes affection their copper and platinum group element contents, *in* Hedenquist, J. W., Thompson, J. F. H., Goldfarb, R. J., and Richards, J. P., eds., One Hundredth Anniversary Volume - Economic Geology 1905-2005, Society of Economic Geologists, p. 179-213.

Barnes, S.-J., and Picard, C., 1993, The behaviour of platinum-group elements during partial melting, crystal fractionation, and sulphide segregation: an example from the Cape Smith Fold Belt, northern Quebec: Geochimica et Cosmochimica Acta, v. 57, p. 79-87.

Barnes, S.-J., and Ripley, E. M., 2016, Highly siderophile and strongly chalcophile elements in magmatic ore deposits: Reviews in Mineralogy and Geochemistry, v. 81, p. 725-774.

Barnes, S.-J., Gorton, M., and Naldrett, A., 1983, A comparative study of olivine and clinopyroxene spinifex flows from Alexo, Abitibi greenstone belt, Ontario, Canada: Contributions to Mineralogy and Petrology, v. 83, p. 293-308.

Barnes, S.-J., Pagé, P., and Zientek, M., 2020, The Lower Banded series of the Stillwater Complex, Montana: whole-rock lithophile, chalcophile, and platinum-group element distributions: Mineralium Deposita, v. 55, p. 163-186.

Barnes, S. J., Cruden, A. R., Arndt, N., and Saumur, B. M., 2016, The mineral system approach applied to magmatic Ni–Cu–PGE sulphide deposits: Ore Geology Reviews, v. 76, p. 296-316.

Blanks, D. E., Holwell, D. A., Fiorentini, M. L., Moroni, M., Giuliani, A., Tassara, S., González-Jiménez, J. M., Boyce, A. J., and Ferrari, E., 2020, Fluxing of mantle carbon as a physical agent for metallogenic fertilization of the crust: Nature communications, v. 11, p. 1-11.

Boudreau, A., 1992, Volatile fluid overpressure in layered intrusions and the formation of potholes: Australian Journal of Earth Sciences, v. 39, p. 277-287.

Boudreau, A. E., 2016, The Stillwater Complex, Montana–Overview and the significance of volatiles: Mineralogical Magazine, v. 80, p. 585-637.

Brenan, J. M., 2015, Se–Te fractionation by sulfide–silicate melt partitioning: Implications for the composition of mantle-derived magmas and their melting residues: Earth and Planetary Science Letters, v. 422, p. 45-57.

Brügmann, G., Naldrett, A., Asif, M., Lightfoot, P., Gorbachev, N., and Fedorenko, V., 1993, Siderophile and chalcophile metals as tracers of the evolution of the Siberian Trap in the Noril'sk region, Russia: Geochimica et Cosmochimica Acta, v. 57, p. 2001-2018.

Cafagna, F., and Jugo, P. J., 2016, An experimental study on the geochemical behavior of highly siderophile elements (HSE) and metalloids (As, Se, Sb, Te, Bi) in a mss-iss-pyrite system at 650° C: a possible magmatic origin for Co-HSE-bearing pyrite and the role of metalloid-rich phases in the fractionation of HSE: Geochimica et Cosmochimica Acta, v. 178, p. 233-258.

Campbell, I. H., and Barnes, S. J., 1984, A model for the geochemistry of the platinum-group elements in magmatic sulphide deposits: Canadian Mineralogist, v. 22, p. 151-160.

Canali, A.C., Brenan, J.M., and Sullivan, N.A., 2017, Solubility of platinum-arsenide melt and sperrylite in synthetic basalt at 0.1 MPa and 1200° C with implications for arsenic speciation and platinum sequestration in mafic igneous systems: Geochimica et Cosmochimica Acta, v. 216, p. 153-168.

Cox, D., Watt, S. F., Jenner, F. E., Hastie, A. R., and Hammond, S. J., 2019, Chalcophile element processing beneath a continental arc stratovolcano: Earth and Planetary Science Letters, v. 522, p. 1-11.

Dare, S. A., Barnes, S.-J., Prichard, H. M., and Fisher, P. C., 2014, Mineralogy and geochemistry of Cu-rich ores from the McCreedy East Ni-Cu-PGE deposit (Sudbury, Canada): implications for the behavior of platinum group and chalcophile elements at the end of crystallization of a sulfide liquid: Economic Geology, v. 109, p. 343-366.

Distler, V. V., 1994, Platinum Mineralisation of the Noril'sk Deposits, *in* Lightfoot, P. C., and Naldrett, A. J., eds., Proceedings of the Sudbury-Noril'sk symposium, Special Publication no. 5, Ontario Geological Survey, p. 243-262.

Duran, C. J., Barnes, S.-J., Pleše, P., Prašek, M. K., Zientek, M. L., and Pagé, P., 2017, Fractional crystallization-induced variations in sulfides from the Noril'sk-Talnakh mining district (polar Siberia, Russia): Ore Geology Reviews, v. 90, p. 326-351.

Edmonds, M., and Mather, T. A., 2017, Volcanic sulfides and outgassing: Elements, v. 13, p. 105-110.

Edmonds, M., Mather, T. A., and Liu, E. J., 2018, A distinct metal fingerprint in arc volcanic emissions: Nature Geoscience, v. 11, p. 790-794.

Forrest, A., Keller, K., and Schilling, J.-G., 2017, Selenium, tellurium and sulfur variations in basalts along the Reykjanes Ridge and extension over Iceland, from 50 N to 65 N: Interdisciplinary Earth Data Alliance (IEDA), Palisades, NY, doi, v. 10.

Godel, B., González-Álvarez, I., Barnes, S. J., Barnes, S.-J., Parker, P., and Day, J., 2012, Sulfides and sulfarsenides from the rosie nickel prospect, Duketon Greenstone Belt, Western Australia: Economic Geology, v. 107, p. 275-294.

Greaney, A. T., Rudnick, R. L., Helz, R. T., Gaschnig, R. M., Piccoli, P. M., and Ash, R. D., 2017, The behavior of chalcophile elements during magmatic differentiation as observed in Kilauea Iki lava lake, Hawaii: Geochimica et Cosmochimica Acta, v. 210, p. 71-96.

Guo, H., and Audétat, A., 2017, Transfer of volatiles and metals from mafic to felsic magmas in composite magma chambers: an experimental study: Geochimica et Cosmochimica Acta, v. 198, p. 360-378.

Hammerli, J., Spandler, C., and Oliver, N. H., 2016, Element redistribution and mobility during upper crustal metamorphism of metasedimentary rocks: an example from the eastern Mount Lofty Ranges, South Australia: Contributions to Mineralogy and Petrology, v. 171, p. 36.

Hanley, J. J., 2007, The role of arsenic-rich melts and mineral phases in the development of high-grade Pt-Pd mineralization within komatiite-associated magmatic Ni-Cu sulfide horizons at Dundonald Beach South, Abitibi subprovince, Ontario, Canada: Economic Geology, v. 102(2), p. 305-317.

Hattori, K. H., Arai, S., and Clarke, D. B., 2002, Selenium, tellurium, arsenic and antimony contents of primary mantle sulfides: The Canadian Mineralogist, v. 40, p. 637-650.

Helmy, H. M., Ballhaus, C., Berndt, J., Bockrath, C., and Wohlgemuth-Ueberwasser, C., 2007, Formation of Pt, Pd and Ni tellurides: experiments in sulfide–telluride systems: Contributions to Mineralogy and Petrology, v. 153, p. 577-591.

Helmy, H. M., Ballhaus, C., Wohlgemuth-Ueberwasser, C., Fonseca, R. O., and Laurenz, V., 2010, Partitioning of Se, As, Sb, Te and Bi between monosulfide solid solution and sulfide melt–application to magmatic sulfide deposits: Geochimica et Cosmochimica Acta, v. 74, p. 6174-6179.

Helmy, H. M., Ballhaus, C., Fonseca, R. O., and Leitzke, F. P., 2020, Concentrations of Pt, Pd, S, As, Se and Te in silicate melts at sulfide, arsenide, selenide and telluride saturation: evidence of PGE complexing in silicate melts?: Contributions to Mineralogy and Petrology, v. 175, p. 1-14..

Holwell, D. A., Fiorentini, M., McDonald, I., Lu, Y., Giuliani, A., Smith, D. J., Keith, M., and Locmelis, M., 2019, A metasomatized lithospheric mantle control on the metallogenic signature of post-subduction magmatism: Nature communications, v. 10, p. 1-10.

Hu, Z., and Gao, S., 2008, Upper crustal abundances of trace elements: a revision and update: Chemical Geology, v. 253, p. 205-221.

Iacono-Marziano, G., Marecal, V., Pirre, M., Gaillard, F., Arteta, J., Scaillet, B., and Arndt, N. T., 2012, Gas emissions due to magma–sediment interactions during flood magmatism at the Siberian Traps: Gas dispersion and environmental consequences: Earth and Planetary Science Letters, v. 357, p. 308-318.

Iacono-Marziano, G., Ferraina, C., Gaillard, F., Di Carlo, I., Arndt, N. T., 2017, Assimilation of sulfate and carbonaceous rocks: Experimental study, thermodynamic modeling and application to the Noril'sk-Talnakh region (Russia): Ore Geology Reviews, v. 90, p. 399-413.

Jenkins, M. C., and Mungall, J. E., 2018, Genesis of the peridotite zone, Stillwater Complex, Montana, USA: Journal of Petrology, v. 59, p. 2157-2189.

Jenkins, M.C., Mungall, J. E., Zientek, M. L., Holick, P., and Butak, K., 2020, The Nature and Composition of the JM Reef, Stillwater Complex, Montana, USA: Economic Geology, v. 115, p. 1799-1826.

Jenner, F. E., and O'Neill, H. S. C., 2012, Analysis of 60 elements in 616 ocean floor basaltic glasses: Geochemistry, Geophysics, Geosystems, v. 13, Q0200.

Kamenetsky, V. S., and Eggins, S. M., 2012, Systematics of metals, metalloids, and volatiles in MORB melts: effects of partial melting, crystal fractionation and degassing (a case study of Macquarie Island glasses): Chemical Geology, v. 302, p. 76-86.

Kamenetsky, V. S., Chung, S.-L., Kamenetsky, M. B., and Kuzmin, D. V., 2012, Picrites from the Emeishan Large Igneous Province, SW China: a compositional continuum in primitive magmas and their respective mantle sources: Journal of Petrology, v. 53, p. 2095-2113.

Ketris, M., and Yudovich, Y. E., 2009, Estimations of Clarkes for Carbonaceous biolithes: World averages for trace element contents in black shales and coals: International Journal of Coal Geology, v. 78, p. 135-148.

Kinloch, E. D., 1982, Regional trends in the platinum-group mineralogy of the critical zone of the Bushveld Complex, South Africa: Economic Geology, v. 77(6), p. 1328-1347.

Le Vaillant, M., Barnes, S. J., Fiorentini, M. L., Barnes, S.-J., Bath, A., and Miller, J., 2018, Platinum-group element and gold contents of arsenide and sulfarsenide minerals associated with Ni and Au deposits in Archean greenstone belts: Mineralogical Magazine, v. 82, p. 625-647.

Li, Y., and Audétat, A., 2015, Effects of temperature, silicate melt composition, and oxygen fugacity on the partitioning of V, Mn, Co, Ni, Cu, Zn, As, Mo, Ag, Sn, Sb, W, Au, Pb, and Bi between sulfide phases and silicate melt: Geochimica Et Cosmochimica Acta, v. 162, p. 25-45.

Liang, Q.-L., Song, X.-Y., Wirth, R., Chen, L.-M., and Dai, Z.-H., 2019, Implications of nano-and micrometer-size platinum-group element minerals in base metal sulfides of the Yangliuping Ni-Cu-PGE sulfide deposit, SW China: Chemical Geology, v. 517, p. 7-21.

Lightfoot, P. C., and Keays, R. R., 2005, Siderophile and chalcophile metal variations in flood basalts from the Siberian trap, Noril’sk region: Implications for the origin of the Ni-Cu-PGE sulfide ores: Economic Geology, v. 100, p. 439-462.

Lightfoot, P., Hawkesworth, C., Hergt, J., Naldrett, A., Gorbachev, N., Fedorenko, V., and Doherty, W., 1993, Remobilisation of the continental lithosphere by a mantle plume: major-, trace-element, and Sr-, Nd-, and Pb-isotope evidence from picritic and tholeiitic lavas of the Noril'sk District, Siberian Trap, Russia: Contributions to Mineralogy and Petrology, v. 114, p. 171-188.

Liu, Y., and Brenan, J., 2015, Partitioning of platinum-group elements (PGE) and chalcogens (Se, Te, As, Sb, Bi) between monosulfide-solid solution (MSS), intermediate solid solution (ISS) and sulfide liquid at controlled *f*O 2–*f*S 2 conditions: Geochimica et Cosmochimica Acta, v. 159, p. 139-161.

Lodders, K., 2003, Solar system abundances and condensation temperatures of the elements: Astrophysical Journal, v. 591, p. 1220-1247.

Lyubetskaya, T., and Korenaga, J., 2007, Chemical composition of Earth's primitive mantle and its variance: 1. Method and results: Journal of Geophysical Research: Solid Earth (1978–2012), v. 112., B03211

Maciag, B. J., and Brenan, J. M., 2020, Speciation of arsenic and antimony in basaltic magmas: Geochimica et Cosmochimica Acta, v. 276, p. 198-218.

Maier, W. D., Barnes, S.-J., and Marsh, J. S., 2003, The concentrations of the noble metals in Southern African flood-type basalts and MORB: implications for petrogenesis and magmatic sulphide exploration: Contributions to Mineralogy and Petrology, v. 146, p. 44-61

Maier, W. D., Barnes, S. J., Campbell, I. H., Fiorentini, M. L., Peltonen, P., Barnes, S.-J., and Smithies, R. H., 2009, Progressive mixing of meteoritic veneer into the early Earth's deep mantle: Nature, v. 460, p. 620-623.

Maier, W., Barnes, S.-J., and Groves, D., 2013, The Bushveld Complex, South Africa: formation of platinum–palladium, chrome-and vanadium-rich layers via hydrodynamic sorting of a mobilized cumulate slurry in a large, relatively slowly cooling, subsiding magma chamber: Mineralium Deposita, v. 48, p. 1-56.

Mansur, E. T., and Barnes, S.-J., 2020a, The role of Te, As, Bi, Sn and Sb during the formation of platinum-group-element reef deposits: Examples from the Bushveld and Stillwater Complexes: Geochimica et Cosmochimica Acta, v. 272, p. 235-258.

Mansur, E. T., and Barnes, S.-J., 2020b, Concentrations of Te, As, Bi, Sb and Se in the Marginal Zone of the Bushveld Complex: Evidence for crustal contamination and the nature of the magma that formed the Merensky Reef: Lithos, v. 358-359,

Mansur, E. T., Barnes, S.-J., Duran, C. J., and Sluzhenikin, S. F., 2020a, Distribution of chalcophile and platinum-group elements among pyrrhotite, pentlandite, chalcopyrite and cubanite from the Noril'sk-Talnakh ores: Implications for the formation of platinum-group minerals: Mineralium Deposita, v. 55, p. 1215-1232.

Mansur, E. T., Barnes, S. J., Savard, D., and Webb, P. C., 2020b, Determination of Te, As, Bi, Sb and Se (TABS) in Geological Reference Materials and GeoPT Proficiency Test Materials by Hydride Generation-Atomic Fluorescence Spectrometry (HG-AFS): Geostandards and Geoanalytical Research, v. 44, p. 147-167.

Marsh, J., Hooper, P., Rehacek, J., Duncan, R., and Duncan, A., 1997, Stratigraphy and age of Karoo basalts of Lesotho and implications for correlations within the Karoo igneous province: Geophysical Monograph-American Geophysical Union, v. 100, p. 247-272

Mather, T. A., 2015, Volcanoes and the environment: Lessons for understanding Earth's past and future from studies of present-day volcanic emissions: Journal of Volcanology and Geothermal Research, v. 304, p. 160-179.

McDonough, W. F., and Arevalo Jr, R., 2008, Uncertainties in the composition of Earth, its core and silicate sphere: Journal of Physics: Conference Series, 2008, p. 022006.

Naldrett, A. J., 2011, Fundamentals of magmatic sulfide deposit, *in* Li, C., and Ripley, E. M., eds., Magmatic Ni-Cu and PGE deposits: Geology, Geochemistry, and Genesis: Society of Economic Geologists, p. 1-50.

Palme, H., and O'Neill, H. St. C., 2014, Cosmochemical estimates of mantle composition., *in* Carlson, R. W., ed., Treatise on Geochemistry, Vol. 3., Elsevier, p. 1–39

Patten, C., Barnes, S-J., Mathez, E.A., and Jenner, F.E., 2013, Partition coefficients of chalcophile elements between sulfide and silicate melts and the early crystallization history of sulfide liquid: LA-ICP-MS analysis of MORB sulfide droplets: Chemical Geology, v. 358, p. 170-188.

Patten, C.G., Pitcairn, I.K., and Teagle, D.A.H., 2017, Hydrothermal mobilisation of Au and other metals in supra-subduction oceanic crust: Insights from the Troodos ophiolite:Ore Geology Reviews, v. 86, p. 487-508.

Picard, C., Lamothe, D., Piboule, M., and Oliver, R., 1990, Magmatic and geotectonic evolution of a Proterozoic oceanic basin system: The Cape Smith thrust-fold belt (New-Quebec): Precambrian Research, v. 47(3-4), p. 223-249.

Piña, R., Gervilla, F., Barnes, S-J., Ortega, L., and Lunar, R., 2013, Partition coefficients of platinum group and chalcophile elements between arsenide and sulfide phases as determined in the Beni Bousera Cr-Ni mineralization (North Morocco): Economic Geology, v. 108(5), p. 935-951.

Piña, R., Gervilla, F., Barnes, S-J., Ortega, L., and Lunar, R., 2015, Liquid immiscibility between arsenide and sulfide melts: evidence from a LA-ICP-MS study in magmatic deposits at Serranía de Ronda (Spain): Mineralium Deposita, v. 50(3), p. 265-279.

Pitcairn, I. K., Craw, D., and Teagle, D. A., 2015, Metabasalts as sources of metals in orogenic gold deposits: Mineralium Deposita, v. 50, p. 373-390.

Pokrovski, G. S., Borisova, A. Y., and Bychkov, A. Y., 2013, Speciation and transport of metals and metalloids in geological vapors: Reviews in Mineralogy and Geochemistry, v. 76, p. 165-218.

Roberts, M., Reid, D., Miller, J., Basson, I., Roberts, M., and Smith, D., 2007, The Merensky Cyclic Unit and its impact on footwall cumulates below Normal and Regional Pothole reef types in the Western Bushveld Complex: Mineralium Deposita, v. 42, p. 271-292.

Samalens, N., Barnes, S-J., and Sawyer, E.W., 2017, The role of black shales as a source of sulfur and semimetals in magmatic nickel-copper deposits: Example from the Partridge River Intrusion, Duluth Complex, Minnesota, USA: Ore Geology Reviews, v. 81(1), p. 173-187.

Shellnutt, J.G., 2013, The Emeishan large igneous province: a synthesis: Geoscience Frontiers, v. 5, p. 369-394.

Shevko, E.P., Bortnikova, S.B., Abrosimova, N.A., Kamenetsky, V.S., Bortnikova, S.P., Panin, G.L., and Zelenski M., 2018, Trace elements and minerals in fumarolic sulfur: the case of Ebeko volcano, Kurile: Geofluids p. 16.

Sinyakova, E., Kosyakov, V., Borisenko, A., 2017, Effect of the presence ofAs, Bi, and Te on the behavior of Pt metals during fractionation crystallization of sulfide magma: Doklady Earth Sciences, v. 477, p.1422–1425.

Sluzhenikin, S. F., Krivolutskaya, N. A., Rad’ko, V. A., Malitch, K. N., Distler, V. A., and Fedorenko, V. A., 2014, Ultramafic-mafic intrusions, volcanic rocks and PGE-Cu-Ni sulfide deposits of the Noril’sk Province, Polar Siberia, *in* Field trip guidebook, 12th International Platinum Symposium Yekaterinburg, p. 80.

Steele, T. W., Levin, J., and Copelwitz, I., 1975, Preparation and certification of a reference sample of a precious metal ore: National Institute for Metallurgy, p. 1696-1975.

Stucker, V. K., Walker, S. L., de Ronde, C. E., Caratori Tontini, F., and Tsuchida, S., 2017, Hydrothermal Venting at Hinepuia Submarine Volcano, Kermadec Arc: Understanding Magmatic-Hydrothermal Fluid Chemistry: Geochemistry, Geophysics, Geosystems, v. 18(10), p. 3646-3661.

Viljoen, M., 1999, The nature and origin of the Merensky Reef of the western Bushveld Complex based on geological facies and geophysical data: South African Journal of Geology, v. 102, p. 221-239.

Wang, H. S., Lineweaver, C. H., and Ireland, T. R., 2018, The elemental abundances (with uncertainties) of the most Earth-like planet: Icarus, v. 299, p. 460-474.

Wieser, P., Jenner, F., Edmonds, M., Maclennan, J., and Kunz, B., 2020, Chalcophile elements track the fate of sulfur at Kīlauea Volcano, Hawai'i: Geochimica et Cosmochimica Acta, v. 282, p. 245-275.

Wilson, A. H., 2012, A Chill Sequence to the Bushveld Complex: Insight into the First Stage of Emplacement and Implications for the Parental Magmas: Journal of Petrology, v. 53, p. 1123-1168.

Wood, B. J., Smythe, D. J., and Harrison, T., 2019, The condensation temperatures of the elements: a reappraisal: American Mineralogist: Journal of Earth and Planetary Materials, v. 104, p. 844-856.

Yi, W., Halliday, A.N., Alt, J.C., Lee, D.C., Rehkämper, M., Garcia, M.O., and Su, Y., 2000, Cadmium, indium, tin, tellurium, and sulfur in oceanic basalts: Implications for chalcophile element fractionation in the Earth: Journal of Geophysical Research: Solid Earth, v. 105(B8), p. 18927-18948.

Zelenski, M., Malik, N., and Taran, Y., 2014, Emissions of trace elements during the 2012–2013 effusive eruption of Tolbachik volcano, Kamchatka-enrichment factors, partition coefficients and aerosol contribution. Journal of Volcanology and Geothermal Research, v. 285, p. 136-149.

Zhang, L., Ren, Z. Y., Handler, M. R., Wu, Y. D., Zhang, L., Qian, S. P., and Xu, Y. G., 2019, The origins of high-Ti and low-Ti magmas in large igneous provinces, insights from melt inclusion trace elements and Sr-Pb isotopes in the Emeishan large Igneous Province: Lithos, v. 344, p. 122-133.

Zientek, M. L., 2012, Magmatic ore deposits in layered intrusions - Descriptive model for reef-type PGE and contact-type Cu-Ni-PGE deposits: U.S. Geological Survey Open File, 2012-1010, p. 48.

Figure captions

Figure 1 – Location of samples used in this study.

Figure 2 – A) Primitive mantle (Lyubetskaya and Korenaga, 2007) normalized plots illustrating the effects of; sulfide segregation, sulfide accumulation, degassing, partial melting and crystal fractionation. B) Primitive mantle normalized plot of the Bushveld B-1 magma (Mansur and Barnes, 2020b) illustrating the effects of assimilation of continental crustal. Note the negative Nb anomaly and enrichment of As, Sb and Bi relative to the other chalophile elements in black shale (Samalens et al. 2017; Ketris and Yudovich, 2009) and upper continental crust (Hu and Gao, 2008) which are also present in the B-1 magma.

Figure 3 – Median primitive mantle normalized plots of: A) MORB samples, note that all samples are depleted in Te, Pd and Pt and that relative to N-MORB E-MORB shows enrichment in both Th and Nb, but not in the chalcophile elements; B) Basalts from the Cape Smith fold belt, note the flat pattern; C) Komatiites form the Abitibi and Baby-Belleterre Greenstone Belts; D) Komatiites from the Barberton Greenstone Belt; E**)** Picrites and basalts from Emeishan Province; F) Picrites and dolerites from Etendeka Province; G) Picrite and basalts from Karoo Province; H) Basalts from the Siberian Province. Note for all of the rocks from large igneous provinces have negative As, Bi, Te and Se anomalies thought to be the product of degassing.

Figure 4. Mg# versus A) Nb and B) Bi for the Alexo komatiite flows. Note Nb and Mg# show a negative correlation with the olivine rich parts of the flow being depleted in Nb as would be expected during crystal fractionation. In contrast, Bi does not show a coherent pattern.

Figure 5 – Primitive mantle normalized plots comparing models of crustal assimilation with the observed patterns: A) Picrite dike and dolerite from the Etendeka Province and B**)** Picrite and basalts from Tuli (Karoo Province).

Figure 6 – Comparison of primitive mantle normalized patterns of all the picrites. Note also none of the picrites have negative Nb anomalies indicating that the component that enriched the mantle in incompatible lithophile elements was not sedimentary. Furthermore, the level and shape of the patterns for all of the picrites are similar for the chalcophile elements and the level of the patterns is

lower than that of Th and Nb indicating that the component enriching the source in lithophile elements did not enrich the source in chalcophile elements.

Figure 7. Primitive mantle normalized plots of: A) Normal and thin Merensky reef (MR; Bushveld Complex); B) Composite Merensky and Plat reefs (Bushveld Complex); C) JM reef (Stillwater Complex). Data from Mansur and Barnes (2020a) and African Minerals Standards www.amis.co.za /

Figure 8. Primitive mantle normalized plots of: A) Cu-poor B) Cu-rich and C) Transitional ore from Talnakh and Kharaelakh intrusions and D) Cu-rich and transitional ore from the Noril'sk 1 intrusion. Data from Duran et al. (2017).

Table caption

Table 1 – Median Values of Chalcophile Elements, Th, Nb and Mg# for studied rocks.

Table 2 – Estimations of TABS concentrations in komatiites and in large igneous provinces picrites.

Online resources – Data availability

Appendicies

Appendix 1 Sample descriptions and analytical methods

Appendix 2 *Table A1* – Analyses of reference materials used to monitor the data quality of HG-AFS analyses. *Table A2* – Analyses of reference materials used to monitor the data quality of whole-rock analyses. *Table A3* – Whole-rock results obtained in this study and compiled from previous studies.

Appendix 3 *Figure A1* – Primitive mantle normalized Th, Nb, Cu, TABS, Pd and Pt plots: **A** high-Ti picrites – Emeishan Province; **B** low-Ti picrites – Emeishan Province; **C** Subvolcanic sill – Emeishan Province; **D** basalts – Emeishan Province; **E** Lesotho Formation – Karoo Province; **F** Barkly East Formation – Karoo Province; **G** Tuli Formation – Karoo Province; **H** Siberian Traps.

Primitive mantle values from Lyubetskaya and Korenaga (2007) *Figure A2* – Primitive mantle normalized Th, Nb, Cu, TABS, Pd and Pt plots: **A** Alexo – Abitibi Greenstone belt **B** Cape Smith belt; **C** Baby Formation; Primitive mantle values from Lyubetskaya and Korenaga (2007)

Table 1 Median Values of Chalcophile Elements, Th, Nb and Mg# for Rocks Presented in This Study

Location or Province	Formation or Location	Rock type	n	As ppm	Se ppm	Sb ppm	Te ppm	Bi ppm	S ppm	Cu ppm	Pd ppb	Pt ppb	Nb ppm	Th ppm	Mg#
MORB															
South Atlantic Ridge		N MORB	6	0.157	0.222	0.019	0.008	0.007	1264	79	0.32	0.05	1.5	0.22	0.63
Hotu Sea Mount		E MORB	2	0.188	0.226	0.020	0.007	0.010	1229	85	0.79	0.35	22.5	0.9	0.58
Garret fracture zone		N MORB	3	0.161	0.225	0.019	0.009	0.010	1167	76	0.35	0.18	4.6	0.18	0.65
Cape Smith	cycle d + e	MORB like	4	0.327	0.301	0.068	0.026	0.053	250	110	12.42	14.07	3.9	0.33	0.61
Komatiites															
Abitibi	Alexo	Spinifex	8	0.405	0.164	0.201	0.020	0.053	450	46	10.09	10.25	0.5	0.06	0.84
Abitibi	Alexo	B2	6	0.266	0.137	0.190	0.014	0.019	500	34	6.77	8.36	0.4	0.05	0.86
Belletere	Baby	Pillows and massive	9	0.836	0.098	0.186	0.007	0.028	349	20	14.00	14.00	1.5	0.05	0.79
Barberton	Komati	Spinifex	2	0.668	0.056	0.147	0.007	0.023	147	31	7.06	5.97	1.9	0.26	0.80
Barberton	Sandspruit	Spinifex	2	1.260	0.024	0.142	<0.005	0.013	n.d.	5	2.72	2.44	1.4	0.15	0.83
Barberton	Hooggenog	Spinifex	2	0.707	0.034	0.127	<0.005	0.019	n.d.	104	4.73	4.72	4.3	1.15	0.75
Picrites															
Emeishan	Daju	High-Ti	6	0.308	0.023	0.073	<0.005	0.010	247	103	2.79	6.78	14.8	1.61	0.78
Emeishan	Shiman	High-Ti	2	0.340	0.024	0.071	<0.005	0.022	139	104	3.42	9.67	15.2	1.6	0.78
Emeishan	Jianchuan	High-Ti	7	0.263	0.038	0.084	0.008	0.007	64	106	7.04	8.35	16.8	1.86	0.76
Emeishan	Dali	Low-Ti	4	0.219	0.046	0.063	0.008	0.039	40	124	5.78	7.17	4.8	0.68	0.77
Emeishan	Binchuan	Low-Ti	5	0.636	0.014	0.094	<0.005	0.014	40	101	5.79	7.81	11.7	2.04	0.80
Etendeka	Horingbaai	Low-Ti	1	0.044	0.040	0.054	<0.005	0.023	150	99	7.00	6.00	4.9	0.65	0.77
Etendeka	Tafelberg	Low-Ti	2	0.198	0.107	0.092	0.019	0.034	505	88	12.00	8.00	4.5	n.a.	0.74
Karoo	Tuli	High-Ti	1	0.502	0.029	0.105	<0.005	<0.005	580	72	4.00	9.00	14.9	2.29	0.74
Basalts and Dolerites															
Emeishan	all 5 localities	Hi-Ti basalt	9	0.392	0.028	0.099	<0.005	<0.005	40	140	6.63	7.82	26.2	2.31	0.60
Etendeka	Horingbaai	Lo-Ti dolerite	2	0.270	0.121	0.076	0.017	0.050	265	239	15.00	6.00	14.0	1.74	0.53
Etendeka	Tafelberg	Lo-Ti dolerite	1	2.076	0.157	0.236	0.024	0.076	650	249	10.00	6.00	11.8	4.77	0.35
Karoo	Lesotho	Lo-Ti basalt	12	0.350	0.031	0.088	<0.005	<0.005	130	97	6.00	5.00	6.8	1.52	0.52
Karoo	Barkly East	Lo-Ti basalt	9	0.590	0.050	0.119	0.008	0.018	254	133	3.50	2.00	6.0	2.05	0.56
Karoo	Tuli	Hi-Ti basalt	2	0.948	0.037	0.151	0.010	0.025	40	281	13.00	8.00	18.0	3.53	0.44
Siberia	Nd	Lo-Ti basalt	2	0.617	0.041	0.185	<0.005	0.029	193	73	0.37	0.50	8.1	3.53	0.56
Siberia	Mr-Kh	Lo-Ti basalt	3	0.368	0.103	0.157	0.009	<0.005	110	238	9.99	10.05	5.1	1.32	0.56
Miscellaneous															
Emeishan	Ertan	Hi-Ti sill	3	0.418	0.035	0.095	<0.005	<0.005	88	87	7.95	18.81	25.9	3.55	0.77
Siberia	Medvezhy Ruchei open pit	Shale	1	10.922	0.031	0.397	0.008	0.127	730	154	4.27	1.67	22.7	19.29	0.52
SARM-7	Bushveld	Merensky reef composite	1	1.38	2.44	1.62	0.62	0.64	4170	700	1542	3700	1.0	1	0.77
ECBV109	Bushveld	Hornfels sediment	1	4.88	0.068	0.82	0.006	0.032	<40	14	nd	nd	12.4	16.2	0.58
n = number of samples	n.d = not determined														

Table 2	Estimations of TABS concentrations in komatiites and LIPS picrites.							
Element	As	Sb	Bi	Cu	Se	Te	Pd	Pt
units	ppm	ppm	ppm	ppm	ppm	ppm	ppb	ppb
Al-undepleted komatiites	0.1*	0.014*	0.008*	46+	0.16+	0.02+	10+	10+
Lo-Ti picrites	0.5*	0.08#	0.03#	103#	0.26#	0.01#	7.2#	7.6#
Hi-Ti picrite	0.5*	0.08#	0.03#	96#	0.26#	0.006#	4.3#	8.7#

*=estimate based on mantle normalization

+ = average of Alexo spinifex for komatiites; # = average of picrites

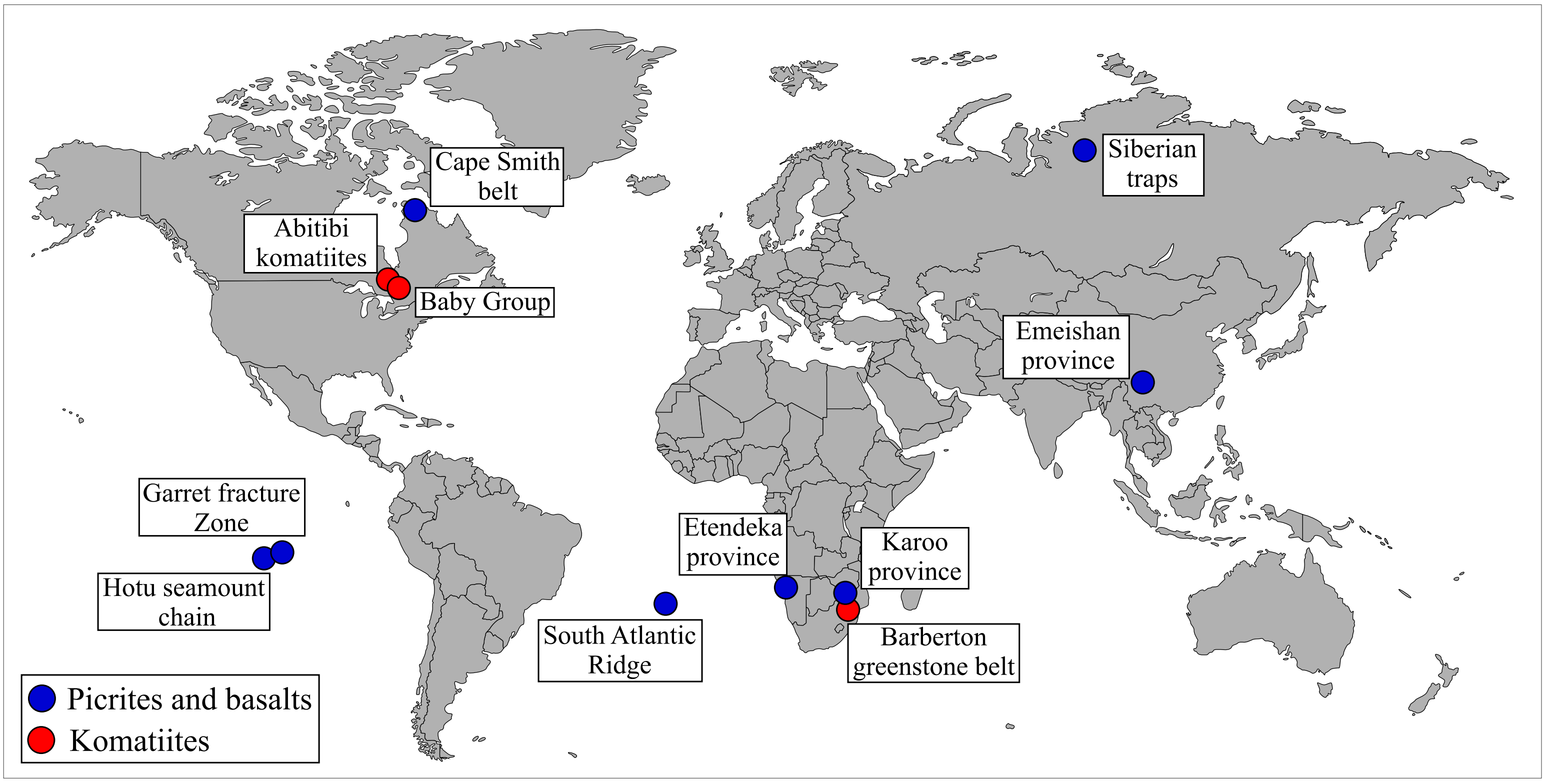
Cape Smith
belt
Siberian
traps
Abitibi
komatiites
Baby Group
Emeishan
province
Garret fracture
Zone
Hotu seamount
chain
Etendeka
province
Karoo
province
South Atlantic
Ridge
Barberton
greenstone belt
Picrites and basalts
Komatiites

Fig.1

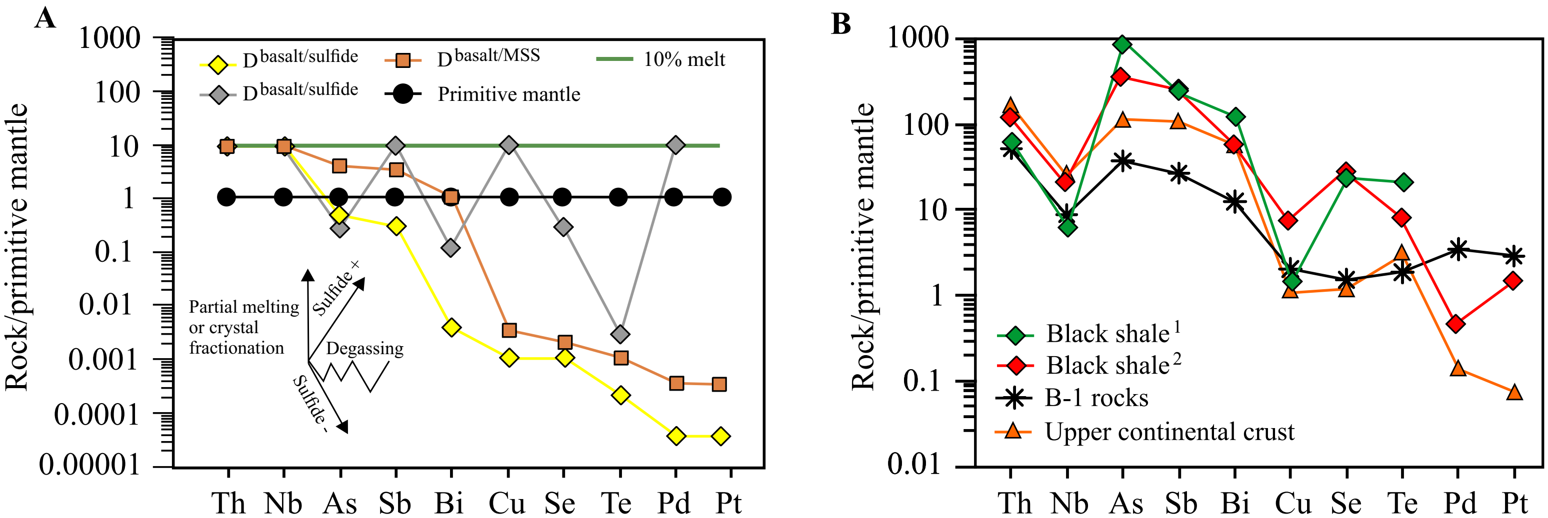
A
Rock/primitive mantle
1000
100
10
1
0.1
0.01
0.001
0.0001
0.00001
D basalt/sulfide
D basalt/sulfide
D basalt/MSS
Primitive mantle
10% melt
Partial melting
or crystal
fractionation
Sulfide +
Degassing
Sulfide -
Th
Nb
As
Sb
Bi
Cu
Se
Te
Pd
Pt
B
Black shale 1
Black shale 2
B-1 rocks
Upper continental crust

Fig. 2

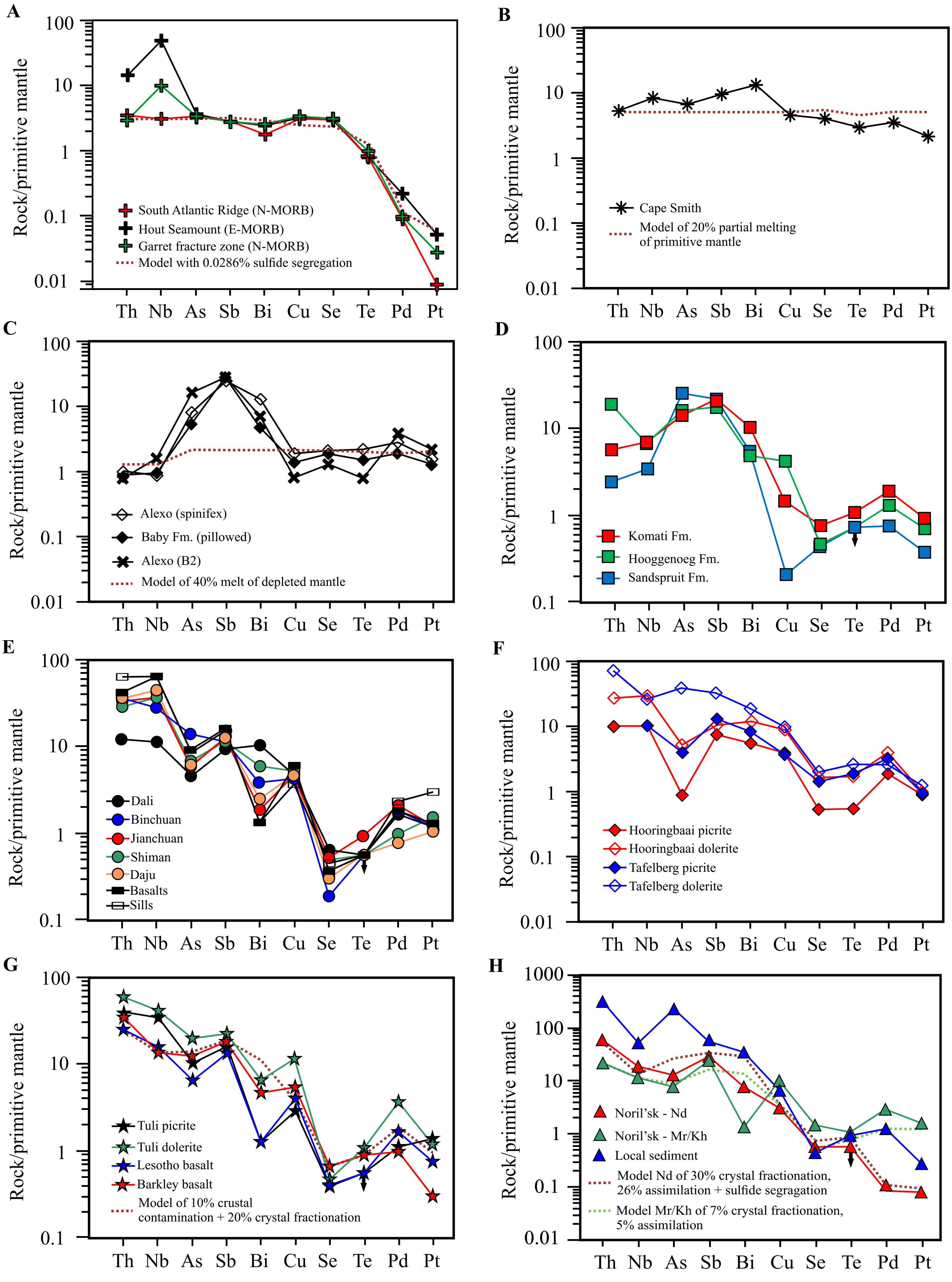
A
B
C
D
E
F
G
H
Rock/primitive mantle
Th Nb As Sb Bi Cu Se Te Pd Pt
100
10
1
0.1
0.01
1000
South Atlantic Ridge (N-MORB)
Hout Seamount (E-MORB)
Garret fracture zone (N-MORB)
Model with 0.0286% sulfide segregation
Cape Smith
Model of 20% partial melting of primitive mantle
Alexo (spinifex)
Baby Fm. (pillowed)
Alexo (B2)
Model of 40% melt of depleted mantle
Komati Fm.
Hooggenoeg Fm.
Sandspruit Fm.
Dali
Binchuan
Jianchuan
Shiman
Daju
Basalts
Sills
Hooringbaai picrite
Hooringbaai dolerite
Tafelberg picrite
Tafelberg dolerite
Tuli picrite
Tuli dolerite
Lesotho basalt
Barkley basalt
Model of 10% crustal contamination + 20% crystal fractionation
Noril'sk - Nd
Noril'sk - Mr/Kh
Local sediment
Model Nd of 30% crystal fractionation, 26% assimilation + sulfide segragation
Model Mr/Kh of 7% crystal fractionation, 5% assimilation

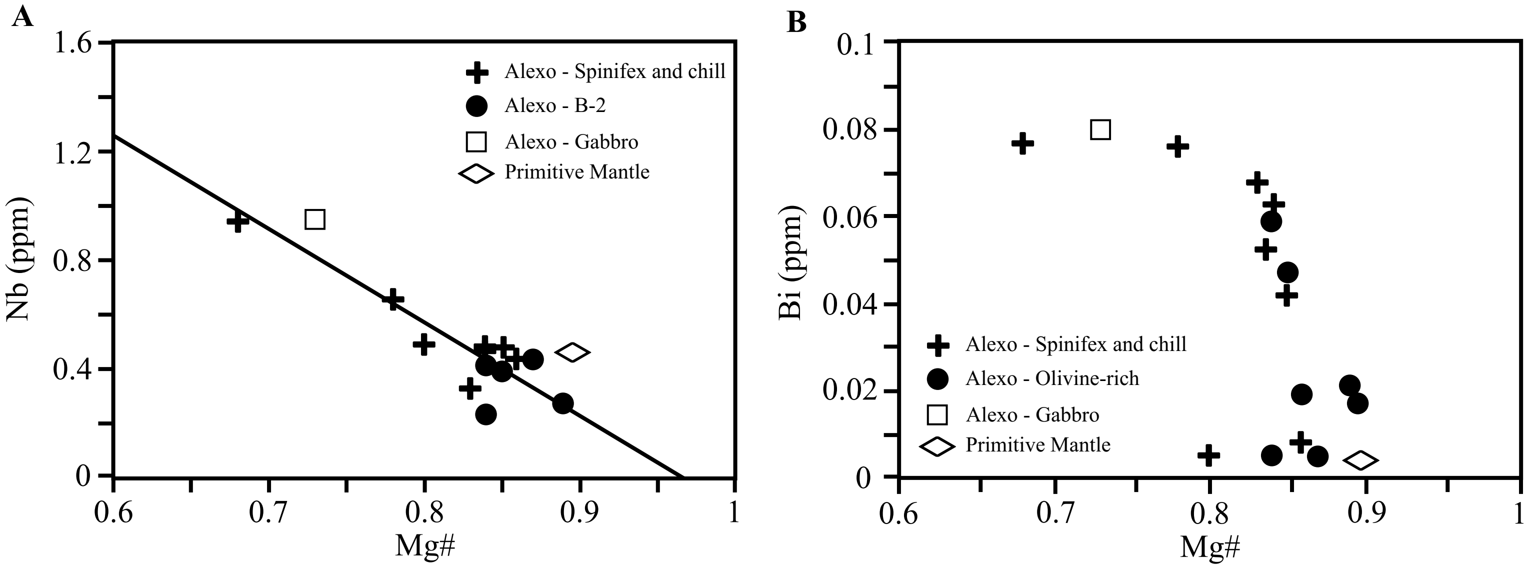
A
1.6
1.2
0.8
0.4
0
Nb (ppm)
0.6
0.7
0.8
0.9
1
Mg#
Alexo - Spinifex and chill
Alexo - B-2
Alexo - Gabbro
Primitive Mantle
B
0.1
0.08
0.06
0.04
0.02
0
Bi (ppm)
Alexo - Spinifex and chill
Alexo - Olivine-rich
Alexo - Gabbro
Primitive Mantle

Fig. 4

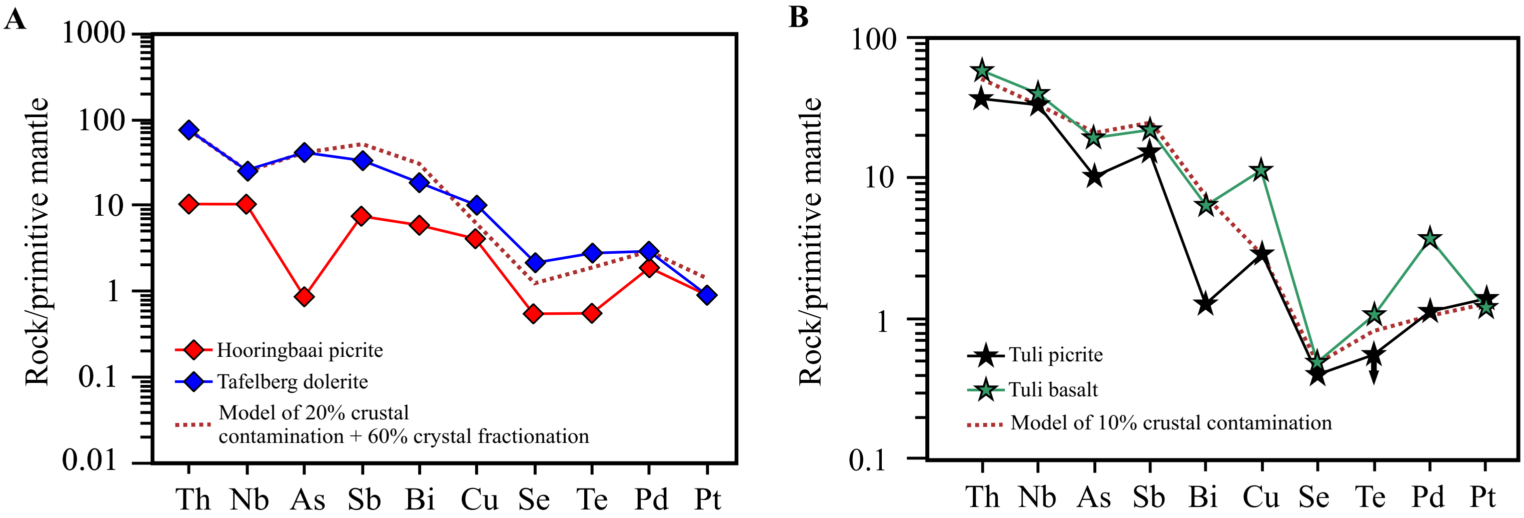
A
1000
100
10
1
0.1
0.01
Rock/primitive mantle
Hooringbaai picrite
Tafelberg dolerite
Model of 20% crustal contamination + 60% crystal fractionation
Th Nb As Sb Bi Cu Se Te Pd Pt
B
100
10
1
0.1
Rock/primitive mantle
Tuli picrite
Tuli basalt
Model of 10% crustal contamination
Th Nb As Sb Bi Cu Se Te Pd Pt

Fig. 5

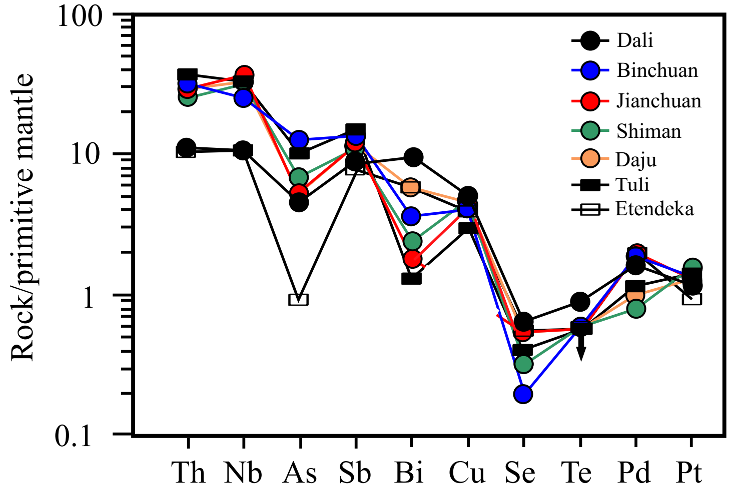

100
10
1
0.1
Rock/primitive mantle
Th
Nb
As
Sb
Bi
Cu
Se
Te
Pd
Pt
Dali
Binchuan
Jianchuan
Shiman
Daju
Tuli
Etendeka

Fig. 6

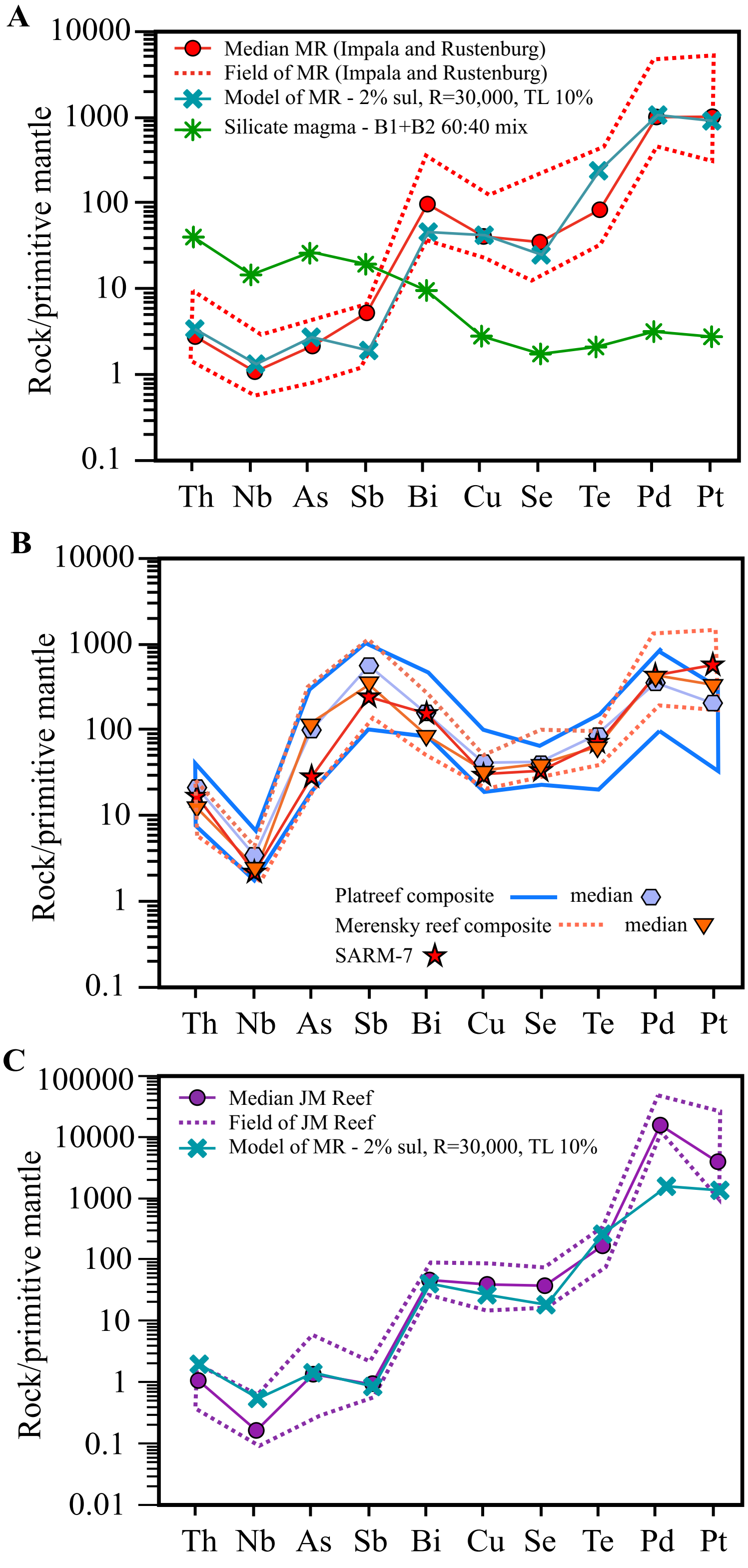
A
10000
1000
100
10
1
0.1
Rock/primitive mantle
Median MR (Impala and Rustenburg)
Field of MR (Impala and Rustenburg)
Model of MR - 2% sul, R=30,000, TL 10%
Silicate magma - B1+B2 60:40 mix
Th
Nb
As
Sb
Bi
Cu
Se
Te
Pd
Pt
B
Platreef composite
median
Merensky reef composite
median
SARM-7
C
100000
0.01
Median JM Reef
Field of JM Reef
Model of MR - 2% sul, R=30,000, TL 10%

Fig. 7

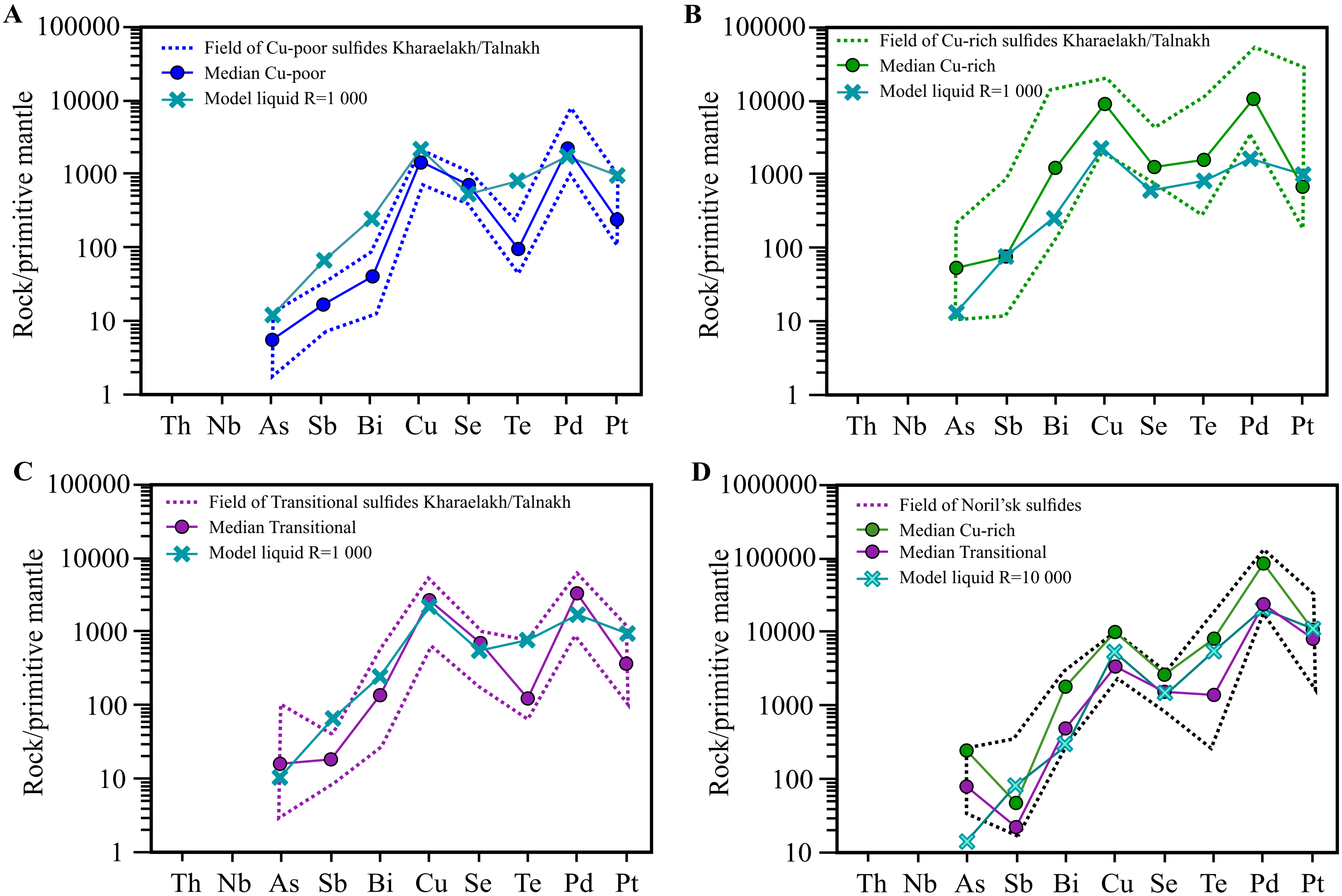
A
Rock/primitive mantle
100000
10000
1000
100
10
1
Field of Cu-poor sulfides Kharaelakh/Talnakh
Median Cu-poor
Model liquid R=1 000
Th Nb As Sb Bi Cu Se Te Pd Pt
B
Field of Cu-rich sulfides Kharaelakh/Talnakh
Median Cu-rich
Model liquid R=1 000
C
Field of Transitional sulfides Kharaelakh/Talnakh
Median Transitional
Model liquid R=1 000
D
1000000
Field of Noril'sk sulfides
Median Cu-rich
Median Transitional
Model liquid R=10 000

Fig. 8

Appendix 1 for Distribution of Te, As, Bi, Sb and Se in; MORB, Komatiites and in Picrites and Basalts from Large Igneous Provinces: Implications for the Formation of Magmatic Ni-Cu-PGE Deposits. Barnes and Mansur (2021) Econ. Geol.

Sample description and Analytical Methods

1. Description of the samples and their geological context

Mid-ocean ridge basalts

We selected 11 MORB samples originally from the repository at the Lamont Doherty Earth Observatory of Columbia University, New York. Six of these are from the South Atlantic Ridge, located between 25°41'S and 26°32'S, whereas the other five are from the East Pacific Rise, two from the Hotu seamount chain and three from the Garrett fracture zone (Fig. 1). The samples were dredged from depths ranging from 2579 to 3999 m, which minimizes S degassing (Mathez, 1976; Patten et al., 2012).

These samples were previously studied by Patten et al. (2012 and 2013). who investigated the textural relations in quenched sulfide droplets, and the partition coefficients of chalcophile elements between sulfide and silicate liquids. The authors argued that the composition of the sulfide droplets was in equilibrium with the silicate glass and that they formed during fractional crystallization of silicate melts in magma chambers beneath the mid-ocean ridges. The seamount samples are LREE enriched and could represent E-MORB, the other samples are LREE depleted and represent N-MORB. These samples are used to examine sulfide segregation.

Cape Smith Belt

The Cape Smith belt is a Proterozoic E-W trending greenstone belt located in northern Quebec, between the Archean Superior and Churchill provinces (Fig. 1). The samples come from the Chukotat Group which consists of olivine-, pyroxene-, and plagioclase-phyric basalts and are interpreted to represent opening of an ocean basin (Picard et al., 1990; Barnes and Picard, 1993; Lesher, 2007). The selected samples are olivine and pyroxene phyric pillow basalts from the cycles d and e of the Chukotat Group and were interpreted as the MORB-like basalts (Hynes and Francis, 1982; Picard et al., 1990). Previous work (Barnes and Picard, 1993) shows that they are not depleted in PGE and hence sulfide segregation or sulfide retention in the source has not occurred. The samples have been metamorphosed to greenschist facies (Picard et al., 1990). The samples should show the effects of partial melting and crystal fractionation without sulfide control, but they could have been altered during metamorphism.

Abitibi Greenstone Belt and the Baby Group

The Abitibi Greenstone Belt is located in the central part of the Superior province, Canada (Fig. 1), occupying an area of approximately 600 km x 300 km, but most of its komatiitic rocks are restricted to the south-west portion of the belt (Ayer et al., 2002; Houlé et al., 2012). The selected samples are Al-undepleted komatiites from the Alexo olivine and clinopyroxene flows and have been previously studied by Barnes et al. (1983), Barnes (1985) and Meric (2018).

The Baby Group is part of the Belletere-Angliers greenstone belt just south of the Abitibi belt (Fig. 1; Dimroth et al., 1983; Barnes et al., 1993; Sawyer and Barnes, 1994). The selected samples were previously studied by Mainville (1994) and are pillowed Al-undepleted komatiites and komatiitic basalts, similar to those from the Abitibi belt.

Both the Alexo and Baby komatiites are undepleted in PGE and thus have not experienced sulfide segregation or sulfide retention in the mantle. The Alexo komatiites have experienced prehnite-pumpellyite facies metamorphism, and the Baby komatiites have experienced greenschist metamorphism and thus both could show some alteration due to metamorphism.

Barberton greenstone belt

The Barberton greenstone belt is a 100 km x 50 km northeast-trending belt of supracrustal igneous and sedimentary rocks located at the eastern border of the Kaapvaal Craton (Fig. 1). The belt represents one of the oldest preserved ultramafic-mafic Archean sequences on the Earth with 3.5 to 3.2 Ga (Zeh et al., 2013). The selected samples are from the ultramafic-mafic basal sequence of the belt, named Onverwatch Group. These comprise 2 samples from each of the Sandspruit, Komati and Hooggenoeg formations. All the samples are Al-depleted spinifex-textured komatiites and were previously studied by Maier et al. (2009), who investigated the PGE distribution in these rocks and concluded that they are depleted in PGE. Although this depletion could be attributed to sulfide segregation Maier et al. (2009) attributed this depletion to the source of the komatiites being depleted in PGE due to incomplete mixing of the later veneer in the primitive mantle. These rocks have experienced greenschist metamorphism and may show evidence of alteration.

Emeishan Large Igneous Province

The Emeishan Large Igneous Province (ELIP) is a continental flood basalt province located in the western margin of the Yangtze craton in SW China (Fig. 1). The province covers an area of ~2.5 x 10^5 km^2, with a total volume of ~0.3 x 10^6 km^3 (Ali et al., 2005; Kamenestky et al., 2012). Geochronology studies shows that the rocks were emplaced around 260 Ma, over an interval of a few million years (Ali et al., 2005; Liu and Zhu, 2009), which is coincident with the end-Guadalupian mass extinction (Zhou et al., 2002; Xu et al., 2008). Several studies interpret the ELIP as having formed by a plume-derived magmatism (Song et al. 2008; Xu et al.2008; Xiao et al., 2004).

The lava sequence ranges in thickness from 200 to more than 5000 m (Shellnutt, 2013) and consists mostly of tholeiitic basalts, which represent more than 95% of the magma volume. Based mainly on their Ti/Y ratios, Xu et al. (2001) classified the tholeiitic basalts of the ELIP into low and high-Ti basalts. The low-Ti basalts have Ti/Y lower than 500, whereas the high-Ti basalts have Ti/Y greater than 500.

The selected samples comprise 15 high-Ti and 9 low-Ti picrite lavass, and 9 flood basalts collected in the Jianchuan, Lijiang (Shiman and Daju sections), Dali and Binchuan, areas, in the western part of the ELI and 3 samples comprising olivine-phyric subvolcanic rocks from the Ertan area. Arguin et al. (2016) previously studied this collection of samples and concluded chromite, olivine and platinum-group mineral crystallization depleted the magma in Os, Ir, Ru and Rh during crystal fractionation, but did not greatly affect Pd or Pt concentrations. These samples are not metamorphosed, but as they are subaerial they may have experienced degassing.

Etendeka Igneous Province

The Etendeka Province is part of the Large Igneous Province denominated Paraná-Etendeka Magmatic Province (PEMP; Peate, et al. 1997; Marsh et al., 2001). The generation of the PEMP is associated with the opening of the South Atlantic Ocean during the Early Cretaceous, around 132 Ma (Renne et al., 1996; Peate, et al. 1997). The Etendeka Province corresponds to the remnant of the associated magmatism in northwest Namibia (Fig. 1), with a present-day outcrop area of approximately 78,000 km^2.

The selected samples consist of 3 dolerite dykes and 3 picritic dykes from the Tafelberg and Horingbaai areas and have been previously studied by Maier et al. (2003), who investigated the distribution of PGE in southern African flood basalts. The Horingbaai dykes represent asthenospheric mantle derived magmas without clear crustal contamination, whereas crustal assimilation is suggested to be more important for Tafelberg dykes (Erlank et al., 1984; Peate and Hawkesworth, 1996; Thompson et al., 2001). Maier et al. (2003) argue that sulfide segregation was not significant during the formation of the rocks from the Etendeka Province. The rocks are not metamorphosed, but they are subvolcanic, and thus could show the effects of degassing and variable degrees of crustal contamination.

Karoo Igneous Province

The Karoo Large Igneous Province is located at the southern part of Africa (Fig. 1) and formed during the separation of the African and Antarctica portions of Gondwana, around 180 Ma (Marsh et al., 1997; Riley and Knight, 2001; McClintock et al., 2008). Most of the remnants of the Karoo province comprise sills intruding sediments of the Karoo Supergroup, and up to 1600 m thick lava pile preserved in the Lesotho region, and a volcanic sequence around the Lebombo–Sabi region (Eales et al., 1984; Duncan et al., 1997; Marsh et al. 1997). Radiometric results show that the emplacement of the lavas took place in a brief event of potentially less than 1 Ma (Jourdan et al., 2007; Svensen et al., 2012).

The samples comprise tholeiitic basalts from the Barkly East (n=8) and Lesotho (n=13) formations, in the southwestern portion of the province, and from the Tuli syncline (n=3) at the northern portion of the province. Strontium isotopic work indicates that the rocks have undergone crustal contamination (Marsh et al., 1997). Based on the PGE content of the lavas Maier et al.

(2003) argued that they have not undergone significant sulfide segregation. The rocks are not metamorphosed, and some are vesicular. They could show the combined effects of degassing and crustal contamination.

Siberian Flood Basalts

The Siberian Large Igneous Province, located across western and eastern Siberia (Fig. 1), comprises very large alkaline, mafic and felsic magmatism erupted at the Permo-Triassic boundary. Geochronology studies shows that the emplacement of the Siberian LIP lasted less than 1 Ma (between 252.3 and 251.3 Ma; Reichow et al., 2009; Burgess et al., 2014). The magmas interacted with the volatile-rich sedimentary rocks, and associated gases released during the Siberian LIP event are believed to be responsible for the end-Permian mass extinction (Polozov et al., 2016, and references therein).

The selected samples are from the Noril'sk region, in the northwest portion of the province, where the full volcanic sequence has been drilled (Fedorenko, 1994). The lower formations were derived from high-Ti magmas with plume characteristics, whereas the upperformations were derived from low-Ti magmas contaminated with continental crust (Lightfoot et al., 1993). The selected samples from the Nadezhdinsky (Nd), Morongovsky (Mr), Mokulaevsky (Mk) and Kharayelakhsky (Kh) formations are part of the upper formations. Additionally, a sample from a shale from the Medvezhy open pit mine was also included as an example of a potential contaminant. Lightfoot et al. (1993) and Brügmann et al. (1993) have shown that the Nd and parts of the Mr formations are depleted in both PGE and Cu and are thought to have segregated a sulfide liquid, with the Nd formation showing the greater degree of contamination. The Nd samples then could show the combined effects of sulfide segregation, degassing and crustal contamination whereas the Mr, Mk and Kh samples should show the effects of degassing and crustal contamination. None of the samples are metamorphosed.

2. Analytical Methods

Tellurium, As, Bi, Sb and Se analyses were carried out by Hydride Generation-Atomic Fluorescence Spectrometry (HG-AFS) following the technique described by Mansur et al. (2020b), at LabMaTer Université du Québec à Chicoutimi (UQAC). Approximately 0.4 g of sample were digested with 5 ml of aqua regia (1:3 HNO_3:HCl) in close-caped beaker at 70ºC for 24 hours. The aliquot was allowed to cool and diluted to 25 ml prior to mixing with a reductant solution (0.7% $NaBH_4$ and 0.4%NaOH). The mixed solution was analysed by Hydride Generation-Atomic Fluorescence Spectrometry (HG-AFS), using a continuous flow PSA Millennium Excalibur 10.055 from PS Analytical. Six calibration solutions with concentrations of 0.1, 0.25, 0.5, 1, 2.5 and 5 ppb were prepared using standard solutions of each element (PlasmaCAL, SCP Science, Quebec, Canada). The calibration solutions were mixed with the reagent blank prior to measurement, in the same proportion as sample aliquots. Calibration solutions were measured at the beginning and the end of each sequence of analysis to monitor fluctuations of the fluorescence signal, which were not observed. International reference materials (CH-4 and TDB-1 from Natural Resources Canada and OKUM from IAGEO), and a blank were determined at the same time as the samples. The detection limits based on 3σ of the blank are 0.005, 0.003, 0.005, 0.005 and 0.002 ppm for Te, As, Bi, Sb and Se, respectively. The results for the reference materials agree with working values (electronic supplementary materials, ESM 3 Table 1).

For most samples, whole-rock analyses were already available in the original publications. For samples where they were not, the samples were analyzed at LabMaTer, (UQAC).

Approximately 0.2g of sample, 1g of flux powder (98.5% $LiBO_2$ and 1.5% LiBr) and 0.2g of NH_4NO_3 were mixed in a platinum crucible and melted using a Claisse Fluxer. The mixture was first heated up to 800ºC for 5 minutes, followed by 4 minutes at 1050ºC and 20 rotations per minute, and finally 3 minutes at 1100ºC and 35 rotations per minute. The melting product is cool down for 3 minutes and a glass disk was produced. The glass disks were mounted in an epoxy block and analysed by laser ablation-inductively coupled plasma-mass spectrometry (LA-ICP-MS). The LA-ICP-MS analyses of the glass disks were performed using an Excimer 193 nm RESOlution M-50 laser ablation system (Australian Scientific Instrument) equipped with a double volume cell S-155 (Laurin Technic) and coupled with an Agilent 7900 mass spectrometer. The LA-ICP-MS tuning parameters were a laser frequency of 10 Hz, a power of 5 mJ/pulse, a dwell time of 7.5 ms, a rastering speed of 5 μm/s, and a fluence of 3 J/cm^2 and a beam size of 80μm. The gas blank was measured for 30s before switching on the laser for at least 60s. The ablated material was carried into the ICP-MS by an Ar–He gas mix at a rate of 0.8–1 L/min for Ar and 350 mL/min for He, and 2mL/min of nitrogen was also added to the mixture. Data reduction was carried out using the Iolite package for Igor Pro software (Paton et al., 2011). The isotopes measured for each element are reported in ESM, Table 2. The certified reference materials OKUM, KPT-1 (IAG reference materials), WPR-1 (CANMET) and UB-N (CNRS-CRPG), were used to monitor the results. The results obtained for the reference materials agree with the working values (ESM 3, Table 2).

References

Ali, J. R., Thompson, G. M., Zhou, M.-F., and Song, X., 2005, Emeishan large igneous province, SW China: Lithos, v. 79, p. 475-489.

Arguin, J.-P., Pagé, P., Barnes, S.-J., Yu, S.-Y., and Song, X.-Y., 2016, The effect of chromite crystallization on the distribution of osmium, iridium, ruthenium and rhodium in picritic magmas:

an example from the Emeishan Large Igneous Province, Southwestern China: Journal of Petrology, v. 57, p. 1019-1048.

Ayer, J., Amelin, Y., Corfu, F., Kamo, S., Ketchum, J., Kwok, K., and Trowell, N., 2002, Evolution of the southern Abitibi greenstone belt based on U–Pb geochronology: autochthonous volcanic construction followed by plutonism, regional deformation and sedimentation: Precambrian Research, v. 115, p. 63-95.

Barnes, S.-J., 1985, The petrography and geochemistry of komatiite flows from the Abitibi Greenstone Belt and a model for their formation: Lithos, v. 18, p. 241-270

Barnes, S.-J., and Picard, C., 1993, The behaviour of platinum-group elements during partial melting, crystal fractionation, and sulphide segregation: an example from the Cape Smith Fold Belt, northern Quebec: Geochimica et Cosmochimica Acta, v. 57, p. 79-87.

Barnes, S.-J., Gorton, M., and Naldrett, A., 1983, A comparative study of olivine and clinopyroxene spinifex flows from Alexo, Abitibi greenstone belt, Ontario, Canada: Contributions to Mineralogy and Petrology, v. 83, p. 293-308.

Barnes, S.-J., Couture, J.-F., Sawyer, E. W., and Bouchaib, C., 1993, Nickel-copper occurrences in the Belleterre-Angliers Belt of the Pontiac Subprovince and the use of Cu-Pd ratios in interpreting platinum-group element distributions: Economic Geology, v. 88, p. 1402-1418.

Burgess, S. D., Bowring, S., and Shen, S.-Z., 2014, High-precision timeline for Earth's most severe extinction: Proceedings of the National Academy of Sciences, v. 111, p. 3316-3321.

Dimroth, E., Imreh, L., Goulet, N., and Rocheleau, M., 1983, Evolution of the south-central segment of the Archean Abitibi belt, Quebec. Part II: Tectonic evolution and geomechanical model: Canadian Journal of Earth Sciences, v. 20, p. 1355-1373.

Duncan, R. A., Hooper, P., Rehacek, J., Marsh, J., and Duncan, A., 1997, The timing and duration of the Karoo igneous event, southern Gondwana: Journal of Geophysical Research: Solid Earth, v. 102, p. 18127-18138.

Eales H.V., Marsh J.S. and Cox K.G. 1984, The Karoo igneous province: An introduction. *In* Erlank, A. J., ed., Petrogenesis of the Volcanic Rocks of the Karoo Province, Geol. Soc. South Africa Spec. Publ. 13, p. l-26.

Erlank, A., Marsh, J., Duncan, A., Miller, R. M., Hawkesworth, C., Betton, P., and Rex, D., 1984, Geochemistry and petrogenesis of the Etendeka volcanic rocks from SWA Namibia. *In* Erlank, A. J., ed., Petrogenesis of the Volcanic Rocks of the Karoo Province, Geol. Soc. South Africa Spec. Publ. 13, p. 195-146.

Fedorenko, V.A. 1994, Evolution of magmatism as reflected in the volcanic sequence of the Noril'sk region. *in* Lightfoot, P. C., and Naldrett, A. J., eds., Proceedings of the Sudbury-Noril'sk symposium, Special Publication no. 5, Ontario Geological Survey p. 171-184.

Houlé, M. G., Lesher, C. M., and Davis, P. C., 2012, Thermomechanical erosion at the Alexo Mine, Abitibi greenstone belt, Ontario: implications for the genesis of komatiite-associated Ni–Cu–(PGE) mineralization: Mineralium Deposita, v. 47, p. 105-128.

Hynes, A., and Francis, D. M., 1982, A transect of the early Proterozoic Cape Smith foldbelt, New Quebec: Tectonophysics, v. 88, p. 23-59

Jourdan, F., Bertrand, H., Schärer, U., Blichert-Toft, J., Féraud, G., and Kampunzu, A., 2007, Major and trace element and Sr, Nd, Hf, and Pb isotope compositions of the Karoo large igneous province, Botswana–Zimbabwe: lithosphere vs mantle plume contribution: Journal of Petrology, v. 48, p. 1043-1077.

Kamenetsky, V. S., Chung, S.-L., Kamenetsky, M. B., and Kuzmin, D. V., 2012, Picrites from the Emeishan Large Igneous Province, SW China: a compositional continuum in primitive magmas and their respective mantle sources: Journal of Petrology, v. 53, p. 2095-2113.

Lesher, C.M., 2007, Ni-Cu-(PGE) Deposits in the Raglan Area, Cape Smith Belt, New Québec, *in* Goodfellow, W. D., ed., Mineral Deposits of Canada: A Synthesis of Major Deposit-Types, District Metallogeny, the Evolution of Geological Provinces, and Exploration Methods: Special Publication No. 5, MineralDeposits Division, Geological Association of Canada, p. 351-386.

Lightfoot, P., Hawkesworth, C., Hergt, J., Naldrett, A., Gorbachev, N., Fedorenko, V., and Doherty, W., 1993, Remobilisation of the continental lithosphere by a mantle plume: major-, trace-element, and Sr-, Nd-, and Pb-isotope evidence from picritic and tholeiitic lavas of the Noril'sk District, Siberian Trap, Russia: Contributions to Mineralogy and Petrology, v. 114, p. 171-188.

Liu C. and Zhu R., 2009, Geodynamic significances of the Emeishan basalts. Frontiers in Earth Science, v. 16, p. 52-69.

Maier, W. D., Barnes, S.-J., and Marsh, J. S., 2003, The concentrations of the noble metals in Southern African flood-type basalts and MORB: implications for petrogenesis and magmatic sulphide exploration: Contributions to Mineralogy and Petrology, v. 146, p. 44-61

Maier, W. D., Barnes, S. J., Campbell, I. H., Fiorentini, M. L., Peltonen, P., Barnes, S.-J., and Smithies, R. H., 2009, Progressive mixing of meteoritic veneer into the early Earth's deep mantle: Nature, v. 460, p. 620-623.

Mainville, M., 1994, Les komatiites et tholeiites a la base du Groupe de Baby, Temiscamingue : Unpub MSc, Université du Québec à Chicoutimi.

Mansur, E. T., Barnes, S. J., Savard, D., and Webb, P. C., 2020, Determination of Te, As, Bi, Sb and Se (TABS) in Geological Reference Materials and GeoPT Proficiency Test Materials by Hydride Generation-Atomic Fluorescence Spectrometry (HG-AFS): Geostandards and Geoanalytical Research, v. 44, p. 147-167.

Marsh, J., Ewart, A., Milner, S., Duncan, A., and Miller, R. M., 2001, The Etendeka Igneous Province: magma types and their stratigraphic distribution with implications for the evolution of the Paraná-Etendeka flood basalt province: Bulletin of Volcanology, v. 62, p. 464-486.

Mathez, E.A., 1976, Sulfur solubility and magmatic sulfides in submarine basalt glass: Journal of Geophysical Research, v. 81, p. 4269-4276.

McClintock, M., White, J.D.L., Houghton, B.F. and Skilling, I.P., 2008, Physical volcanology of a large crater-complex formed during the initial stages of Karoo flood basalt volcanism, Sterkspruit, Eastern Cape, South Africa:Journal of Volcanology and Geothermal Research, v. 172(1-2), p. 93-111.

Meric, J., 2018, Le ruthénium (Ru), iridium (Ir), osmium (Os) et rhodium (Rh) et les éléments traces dans des chromites de komatiites issues de la zone Alexo et de la zone Hart,(Abitibi, Ontario): un outil diagnostique pour l'exploration de systèmes fertiles: Unpub MSc, Université du Québec à Chicoutimi.

Paton, C., Hellstrom, J., Paul, B., Woodhead, J., and Hergt, J. (2011) Iolite: Freeware for the visualisation and processing of mass spectrometric data: Journal of Analytical Atomic Spectrometry, v. 26, p. 2508-2518.

Patten, C., Barnes, S-J., and Mathez, E.A., 2012, Textural variations in MORB sulfide droplets due to differences in crystallization history: The Canadian Mineralogist, v. 50(3), p. 675-692.

Patten, C., Barnes, S-J., Mathez, E.A., and Jenner, F.E., 2013, Partition coefficients of chalcophile elements between sulfide and silicate melts and the early crystallization history of sulfide liquid: LA-ICP-MS analysis of MORB sulfide droplets: Chemical Geology, v. 358, p. 170-188.

Peate, D., and Hawkesworth, C.J., 1996, Lithospheric to asthenospheric transition in low-Ti flood basalts from southern Parana, Brazil: Chemical Geology, v. 127, 1-24.

Peate, D. W., 1997, The Parana-Etendeka Province. *in* Mahoney, J.J. and Coffin, M.F. (eds.) Large Igneous Provinces: Continental, Oceanic, and Planetary Flood Volcanism: American Geophysical Union, Monograph 100, p. 217–245.

Polozov, A.G., Svensen, H.H., Planke, S., Grishina, S.N., Fristad, K.E., and Jerram, D.A., 2016, The basalt pipes of the Tunguska Basin (Siberia, Russia): High temperature processes and volatile degassing into the end-Permian atmosphere: Palaeogeography Palaeoclimatology Palaeoecology, v. 441, p. 51-64.

Reichow, M.K., Pringle, M.S., Al'Mukhamedov, A.I., Allen, M.B., Andreichev, V.L., Buslov, M.M., Davies, C.E., Fedoseev, G.S., Fitton, J.G., Inger, S., Medvedev, A.Y., Mitchell, C., Puchkov, V.N., Safonova, I.Y., Scott, R.A., and Saunders, A.D., 2009, The timing and extent of the eruption of the Siberian traps large igneous province: implications for the end-Permian environmental crisis: Earth and Planetary Science Letters, v. 277, p. 9-20.

Renne, P.R., Glen, J.M., Milner, S.C., and Duncan, A.R., 1996, Age of Etendeka volcanism and associated intrusions in southwestern Africa: Geology, v. 24, p. 659-662.

Riley, T.R., and Knight, K.B., 2001, Age of pre-break-up Gondwana magmatism: Antarctic Science, v. 13(2), p. 99-110.

Sawyer, E.W., and Barnes, S-J., 1994, Thrusting, magmatic intraplating, and metamorphic core complex development in the Archaean Belleterre-Angliers greenstone belt, Superior Province, Quebec, Canada: Precambrian Research, v. 68(3-4), p. 183-200.

Shellnutt, J.G., 2013, The Emeishan large igneous province: a synthesis: Geoscience Frontiers, v. 5, p. 369-394.

Song, X.Y., Qi H.W., Robinson, P.T., Zhou, M.F., Cao, Z.M., and Chen, L.M., 2008, Melting of the subcontinental lithospheric mantle by the Emeishan mantle plume; evidence from the basal alkaline basalts in Dongchuan, Yunnan, Southwestern China: Lithos, v. 100, p. 93-111.

Svensen, H., Corfu, F., Polteau, S., Hammer, Ø., and Planke, S., 2012, Rapid magma emplacement in the Karoo large igneous province: Earth and Planetary Science Letters, v. 325, p. 1-9.

Thompson, R.N., Gibson, S.A., Dickin, A.P., and Smith, P.M., 2001, Early Cretaceous basalt and picrite dykes of the southern Etendeka region, NW Namibia: windows into the role of the Tristan mantle plume in Parana-Etendeka magmatism: Journal of Petrology, v. 42, p. 2049-2081.

Xiao, L., Xu, Y.G., Mei, H.J., Zheng, Y.F., He, B., and Pirajno, F., 2004, Distinct mantle sources of low-Ti and high-Ti basalts from the western Emeishan large igneous province, SW China: implications for plume-lithosphere interaction: Earth and Planetary Science Letters, v. 228, p. 525-546.

Xu, Y., Chung, S. L., Jahn, B. M., and Wu, G., 2001, Petrologic and geochemical constraints on the petrogenesis of Permian–Triassic Emeishan flood basalts in southwestern China: Lithos, v. 58, p. 145-168.

Xu, Y.G., Luo, Z.Y., Huang, X.L., He, B., Xiao, L., Xie, L.W., and Shi, Y.R., 2008, Zircon U-Pb and Hf isotope constraints on crustal melting associated with the Emeishan mantle plume: Geochimica et Cosmochimica Acta, v. 72, p. 3084-3104.

Zeh, A., Gerdes, A., and Heubeck, C., 2013, U–Pb and Hf isotope data of detrital zircons from the Barberton Greenstone Belt: constraints on provenance and Archaean crustal evolution: Journal of the Geological Society of London, v. 170(1), p. 215-223.

Zhou, M.F., Malpas, J., Song, X.Y., Robinson, P.T., Sun, M., Kennedy A.K., and Keays R.R., 2002, A temporal link between the Emeishan large igneous province (SW China) and the end-Guadalupian mass extinction. Earth and Planetary Science Letters, v. 196(3-4), p. 113-122.

READ ME

Online Resource (ESM) for

Distribution of Te, As, Bi, Sb and Se (TABS+) in MORB, Komatiites and in Picrites and Basalts from Large Igneous Provinces: Implications for the Formation of Magmatic Ni-Cu-PGE Deposits

* Sarah-Jane Barnes[1], Eduardo T. Mansur[1]

Economic Geology

[1]Sciences de la Terre, Université du Québec à Chicoutimi, Québec, G7H 2B1, Canada

*Corresponding author - E-mail address: sjbarnes@uqac.ca

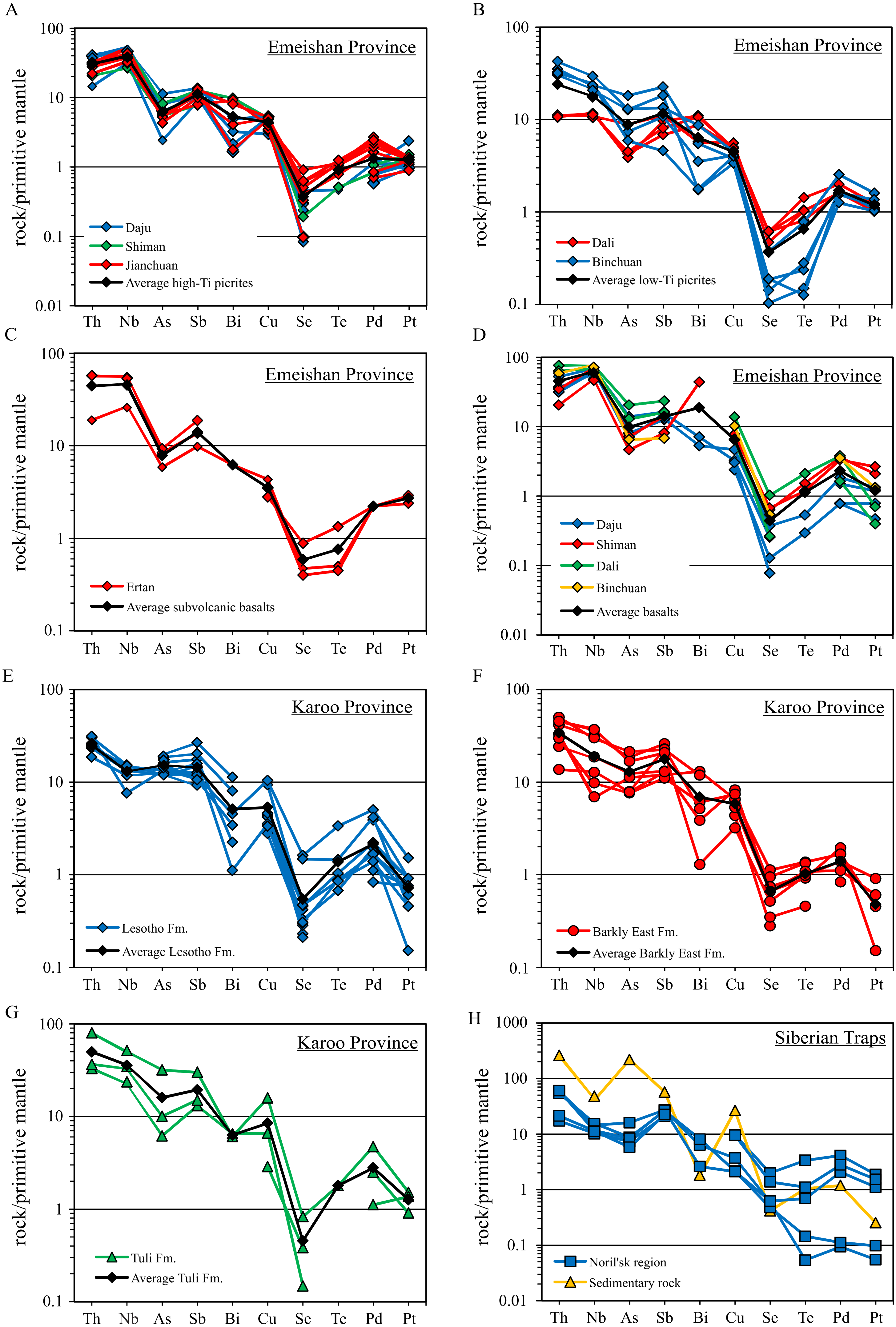

Appendix 3 Fig A1 A high-Ti picrites – Emeishan Province; B low-Ti picrites – Emeishan Province; C Subvolcanic sill – Emeishan Province; D basalts – Emeishan Province; E Lesotho Formation – Karoo Province; F Barkly East Formation – Karoo Province; G Tuli Formation – Karoo Province; H Siberia

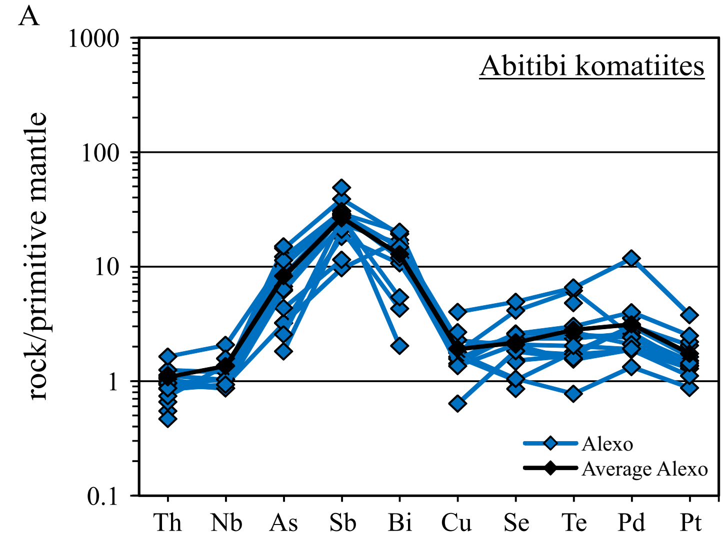

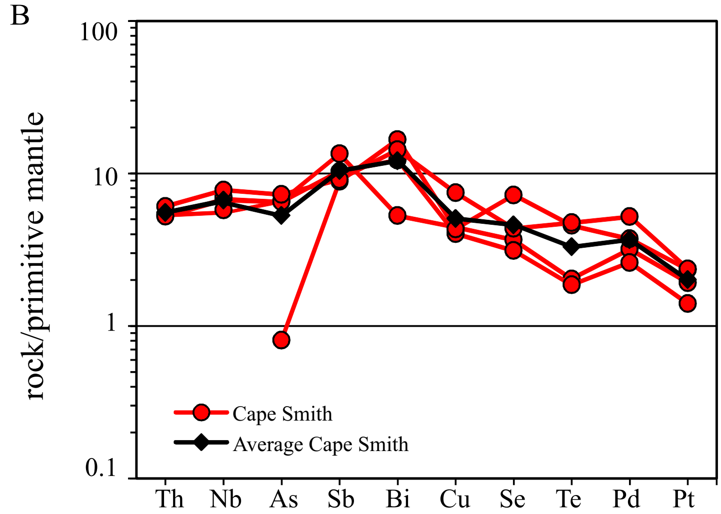

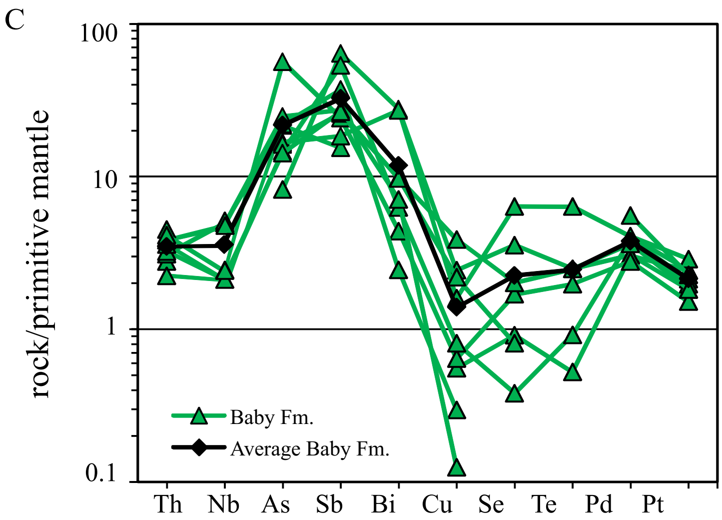

Appendix 3 Barnes and Mansure (2021) Econ Geol
Figure A2 – Primitive mantle normalized Th, Nb, Cu, TABS, Pd and Pt plots: A Alexo – Abitibi Greenstone belt B Cape Smith belt; C Baby Formation; Primitive mantle values from Lyubetskaya and Korenaga (2007)